nature immunology



Article

https://doi.org/10.1038/s41590-024-02041-2

β-Glucan reprograms neutrophils to promote disease tolerance against influenza A virus

Received: 2 August 2023

Accepted: 21 November 2024

Published: 8 January 2025



Nargis Khan ® ^{1,2,10} ⋈, Kim A. Tran ® ^{1,10}, Raphael Chevre³, Veronica Locher⁴, Mathis Richter ® ³, Sarah Sun⁵, Mina Sadeghi ® ¹, Erwan Pernet¹, Andrea Herrero-Cervera ® ³, Alexandre Grant¹, Ahmed Saif¹, Jeffrey Downey¹, Eva Kaufmann¹, Shabaana Abdul Khader ® ⁻, Philippe Joubert³, Luis B. Barreiro ® ⁴, Bryan G. Yipp ® ¸, Oliver Soehnlein ® ³ & Maziar Divangahi ® ¹ ⋈

Disease tolerance is an evolutionarily conserved host defense strategy that preserves tissue integrity and physiology without affecting pathogen load. Unlike host resistance, the mechanisms underlying disease tolerance remain poorly understood. In the present study, we investigated whether an adjuvant (β -glucan) can reprogram innate immunity to provide protection against influenza A virus (IAV) infection. β -Glucan treatment reduces the morbidity and mortality against IAV infection, independent of host resistance. The enhanced survival is the result of increased recruitment of neutrophils via RoRyt⁺T cells in the lung tissue. β -Glucan treatment promotes granulopoiesis in a type 1 interferon-dependent manner that leads to the generation of a unique subset of immature neutrophils utilizing a mitochondrial oxidative metabolism and producing interleukin-10. Collectively, our data indicate that β -glucan reprograms hematopoietic stem cells to generate neutrophils with a new 'regulatory' function, which is required for promoting disease tolerance and maintaining lung tissue integrity against viral infection.

It is increasingly understood that host defense strategies against infectious diseases comprise both host resistance and disease tolerance. Host resistance prevents invasion or eliminates pathogens, whereas disease tolerance limits tissue damage caused by a pathogen and/or the immune response $^{1-3}$. Unlike resistance, disease tolerance does not necessarily exert direct effects on pathogen growth. It plays a critical role in pulmonary infections via promoting tissue-repair mechanisms to maintain lung tissue integrity and function. For instance, we have

recently demonstrated how pulmonary macrophages⁴ or natural killer cells⁵ can promote disease tolerance against influenza A virus (IAV) infection. However, how we can harness the power of disease tolerance against infectious diseases remains largely unknown. The capacity of innate immune cells to maintain memory (trained immunity) has revealed an important and unrecognized property of innate immune responses that can be targeted to enhance host defense against infectious diseases. Although there has been mounting evidence to show

¹Department of Medicine, Department of Pathology, Department of Microbiology & Immunology, McGill University Health Centre, McGill International TB Centre, Meakins Christie Laboratories, McGill University, Montréal, Québec, Canada. ²Calvin, Phoebe and Joan Snyder Institute for Chronic Diseases, Department of Microbiology, Immunology, and Infectious Diseases, Cumming School of Medicine, University of Calgary, Calgary, Alberta, Canada. ³Institute of Experimental Pathology, Centre of Molecular Biology of Inflammation, Münster, Germany. ⁴Committee on Immunology, University of Chicago, Chicago, IL, USA. ⁵Genetics, Genomics, and Systems Biology, University of Chicago, Chicago, IL, USA. ⁶Department of Biomedical and Molecular Sciences, Queen's University, Kingston, Ontario, Canada. ⁷Department of Microbiology, University of Chicago, Chicago, IL, USA. ⁸Department of Molecular Biology, Medical Biochemistry and Pathology, Laval University, Québec City, Québec, Canada. ⁹Calvin, Phoebe and Joan Snyder Institute for Chronic Diseases, Department of Critical Care, Cumming School of Medicine, University of Calgary, Calgary, Alberta, Canada. ¹⁰These authors contributed equally: Nargis Khan, Kim A. Tran. ⊠e-mail: nargis.khan1@ucalgary.ca; maziar.divangahi@mcgill.ca

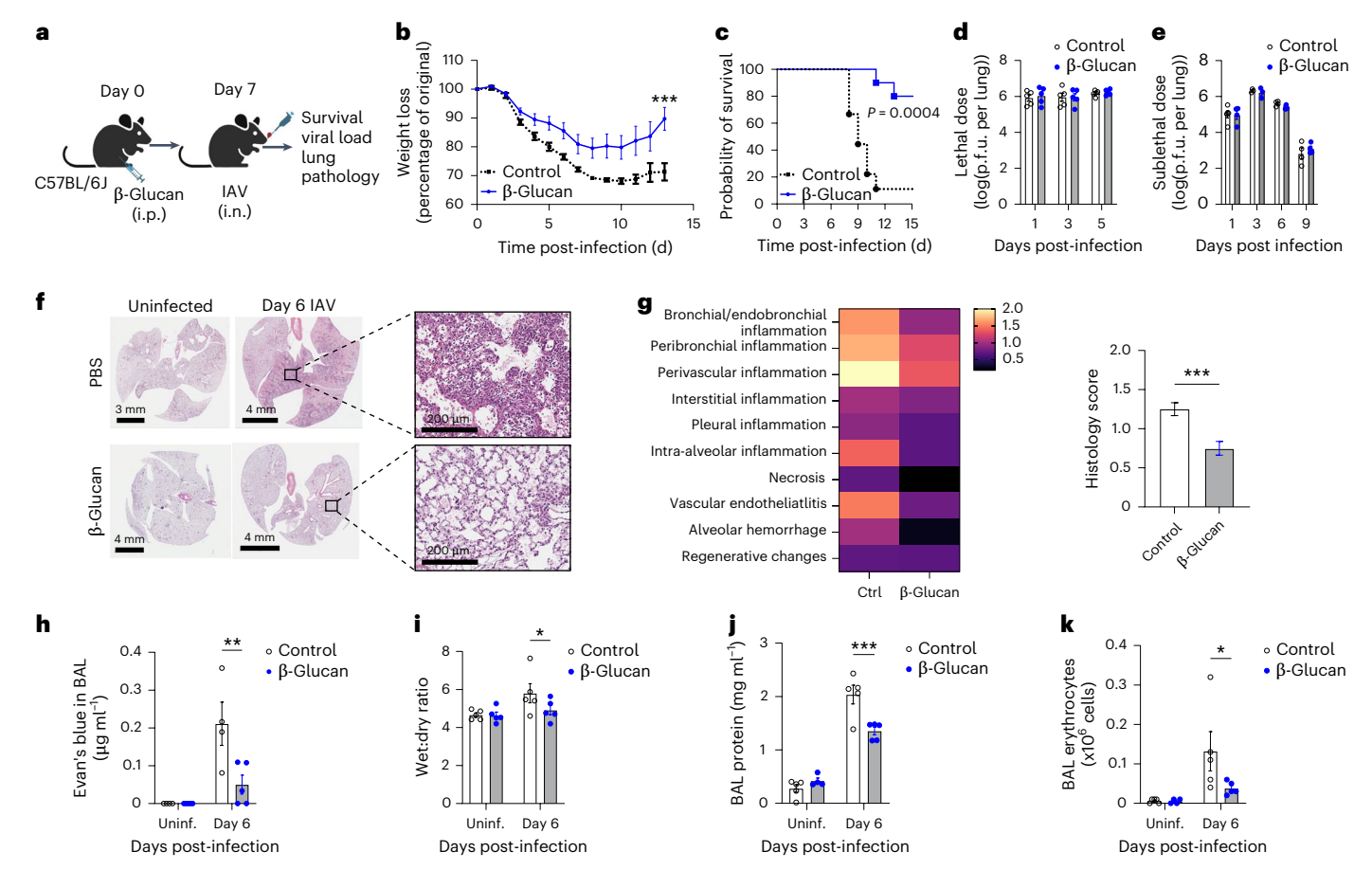


Fig. 1| β-Glucan treatment induces disease tolerance against IAV. a, Mice were infected with IAV at day 7 post-β-glucan treatment i.p. b, c, Weight loss (b) and survival (c) monitored over time (n=10) of mice infected with a lethal dose of IAV (120 p.f.u.). d, Viral burden quantified at several time points post-IAV infection with a lethal dose (n=5). e, Viral burden quantified at several time points post-IAV infection with a sublethal dose (50 p.f.u.; n=5). f, Representative micrographs of lung histology from β-glucan (7 d)-treated mice stained with H&E day 6 post-IAV infection. Scale bar, 200 μm. g, Lung histology scoring at day 6

post-IAV infection after β -glucan treatment (n=5). $\mathbf{h}-\mathbf{k}$, Mice were infected with a sublethal dose of IAV at day 7 post- β -glucan, followed at day 6 post-IAV infection: quantification of endothelial permeability (\mathbf{h}), pulmonary edema (\mathbf{i}), BAL protein (\mathbf{j}) and BAL erythrocytes (\mathbf{k}) (n=5). Data are represented as mean \pm s.e.m. Data were analyzed using two-tailed, unpaired Student's t-test (\mathbf{g}) or two-way ANOVA followed by Šidák's multiple-comparison tests (\mathbf{b} and $\mathbf{h}-\mathbf{k}$). Survival was monitored by a log(rank) test (\mathbf{c}). 'P < 0.001, '"P < 0.001, '"P < 0.0001.i.n., intranasally; uninf., uninfected. Illustrations in \mathbf{a} created using BioRender.com.

that the innate immune system can confer long-term functional reprogramming against homologous or heterologous infections by boosting host resistance 6,7 , little is known about the contribution of innate immune memory responses in promoting disease tolerance. Considering the relatively short lifespan of innate cells, we and others have demonstrated that the maintenance of innate immune memory cells relies on reprogramming the bone marrow hematopoietic stem cells (HSCs) that give rise to progenitor and mature innate immune cells 8 . For instance, β -glucan (a fungal cell wall component) reprograms HSCs and generates trained monocytes promoting host resistance against chronic *Mycobacterium tuberculosis* (*Mtb*) infection, which remarkably enhances host survival 9 . Similarly, β -glucan has been shown to protect against various acute bacterial infections, fungi or tumors 10,11 , but its role against pulmonary viral infection is unclear.

The severity of pulmonary viral infections often reflects lung damage, the dominant feature of fatal outcomes ¹². Immunopathology is attributed to an overexuberant inflammatory response in the airways and lungs, frequently initiated by neutrophil recruitment. Neutrophils are the most abundant cell types, representing 50–70% of the total circulatory leukocytes with a short lifespan (-24 h)¹³. At steady state, neutrophils contribute to tissue repair and homeostasis by phagocytosing necrotic cells and producing resolvins and protectins ¹⁴. It is well established that neutrophils' antimicrobial functions are essential against infections because neutrophil disorders are associated with

recurrent bacterial or fungal infections ¹⁵. However, recent studies have shown that the functional spectrum of neutrophils ranges from programming alveolar macrophages in the developing lung ¹⁶ to limiting tissue damage and promoting wound healing after injury or infection ^{17–19}. Thus, dissection of the cellular and molecular mechanisms imprinting neutrophil heterogeneity may provide an opportunity to harness their power during infections.

Since β -glucan provides protection against bacterial or fungal infections 9,20 , we sought to investigate the impact of β -glucan during IAV infection. In the present study, we show that β -glucan reprograms HSCs and promotes granulopoiesis via type I interferon (IFN) signaling, which gives rise to a unique subset of regulatory neutrophils. These neutrophils exhibit a less mature phenotype with an altered metabolic program and a capacity to produce interleukin-10 (IL-10.) Unlike their classic role in host resistance, β -glucan-mediated regulatory neutrophils promote disease tolerance against IAV via limitation of the lung pathology independent of viral replication.

Results

β-Glucan promotes disease tolerance against IAV infection

Recently, we have demonstrated that β -glucan enhances host resistance against tuberculosis°. To investigate the potential benefit of β -glucan in host defense against pulmonary viral infection, we treated C57BL/6 mice with β -glucan intraperitoneally (i.p.) and, after 7 d, mice

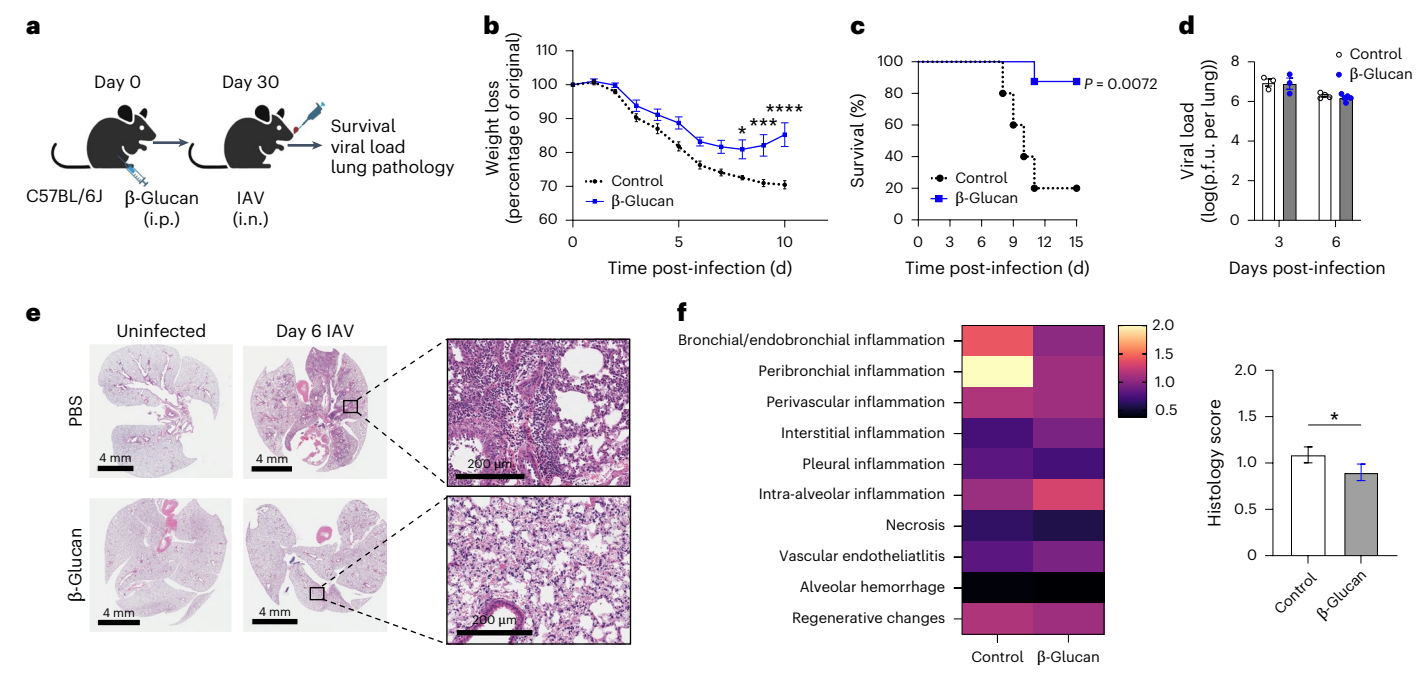


Fig. 2 | β -Glucan treatment promotes long-lasting disease tolerance against IAV infection. a, Mice were infected with IAV with a lethal (survival and weight loss) or sublethal dose (viral load and pathology) at day 30 post- β -glucan treatment i.p. b, c, Weight loss (b) and survival (c) monitored over time (n = 10). d, Viral load quantified at days 3 and 6 post-infection (n = 4). e, Representative micrographs of lung histology from β -glucan (30 d)-treated mice stained with

H&E at day 6 post-IAV infection. Scale bar, 200 μm. **f**, Lung histology at day 6 post-IAV infection after β-glucan long treatment (n = 5-6). Data are represented as mean \pm s.e.m. Data were analyzed using two-tailed, unpaired Student's t-test (f) or two-way ANOVA followed by Šidák's multiple-comparison tests (f and f). Survival was monitored by a log(rank) test (f). f0.005, f0.001, f0.0001. Illustrations in f0.0001.

were infected with IAV (Fig. 1a). With a lethal dose, mice treated with β-glucan showed significantly reduced morbidity and increased survival against IAV (Fig. 1b,c). We quantified the pulmonary viral burden before the onset of mortality and showed that there was no difference in viral load after lethal or sublethal IAV infection (Fig. 1d,e). Although the increased survival of β-glucan mice infected with IAV was independent of host resistance, these mice showed remarkably reduced immunopathology compared with control infected mice at day 6 post-IAV infection (Fig. 1f). The corresponding lung histology demonstrated reduced inflammation (Fig. 1g), which was corroborated with reduced endothelial permeability, pulmonary edema and decreased proteins and erythrocytes in the bronchoalveolar lavage fluid (BAL) of β-glucan-treated mice infected with IAV (Fig. 1h-k). To assess the longevity of β-glucan-mediated protection against IAV, mice were treated with β-glucan and, after 30 d, were infected with IAV (Fig. 2a). Similar to the β-glucan short treatment (7 d), the protective impact of β-glucan on morbidity and mortality against IAV was maintained even after 30 d (Fig. 2b,c). This enhanced host defense was independent of host resistance but dependent on reduced lung immunopathology (Fig. 2d-f). Collectively, these data indicate that β-glucan treatment enhances host defense against IAV by promoting disease tolerance rather than increasing antiviral responses.

β-Glucan increases neutrophil recruitment into the lungs

We have shown that β -glucan trains monocytes and macrophages against Mtb° . In contrast to Mtb, the protection of β -glucan against IAV was independent of pulmonary viral load, but reduced immunopathology, suggesting that β -glucan regulates disease tolerance against IAV. Interestingly, immunophenotyping of β -glucan-treated mice showed a significant increase in the frequency and absolute number of neutrophils in the lungs, which peaked on day 4 and returned to baseline by day 7 (Fig. 3a–d). The identification of neutrophils is based on the expression of surface marker protein Ly6G (Extended Data Fig. 1a,

gating strategy). However, a recent study identified an atypical subset of a Ly6G⁺CD64⁺ macrophage population with a function in tissue repair after IAV infection²¹. We therefore assessed the expression of CD64 in β-glucan-induced pulmonary neutrophils before and after IAV infection (Extended Data Fig. 2a,b). After 4 d of β-glucan treatment, >99% of the cells in our gated neutrophil population were identified as Ly6G⁺CD64⁻ and >90% after 6 d of IAV infection (Extended Data Fig. 2c). These data collectively indicate that the increased number of Ly6G⁺ cells after B-glucan is caused by neutrophils and not macrophages. The differences in other pulmonary myeloid or lymphoid cells, such as monocytes/macrophages or T cells, were minimal (Extended Data Fig. 2d.e). Furthermore, this neutrophilia was not limited to the lungs of β-glucan-treated mice, seeing as the number of neutrophils was also increased in the blood, spleen and peritoneal cavity (Extended Data Fig. 2f-j). Recent studies in neutrophil dynamics suggest that the trafficking of neutrophils from the vasculature into tissue is critical in defining their functions²². Using an intravascular staining technique, we showed that the number of neutrophils was significantly increased in both the lung vasculature and the parenchyma of mice treated with β-glucan (Fig. 3e and Extended Data Fig. 2k). To directly investigate the impact of β-glucan on lung neutrophil recruitment and localization in vivo, pulmonary confocal intravital microscopy was performed in Ly6G-TdTom mice. Intravenously (i.v.) administered, fluorescently conjugated, anti-CD45 monoclonal antibodies were used to differentiate vascular neutrophils from nonvascular neutrophils. Corroborating the flow cytometry data, intravital results also showed β-glucan-induced neutrophil recruitment into the lungs, but these neutrophils were significantly less vascular (Fig. 3f-h). Importantly, the intravascular staining also showed that both the frequency and the absolute numbers of neutrophils in the lung vasculature and parenchyma were increased in β -glucan-treated mice after 6 d of infection with IAV (Fig. 3i-k). This was specific to neutrophils, because there was no difference in the kinetics of other immune cells in the lungs after IAV infection in both

frequency and absolute number (Extended Data Fig. 3a–g). Using IL-10 reporter mice ($Il10^{GFP}$), we found that there was an increased number of Il10-expressing cells after 6 d of IAV infection in β -glucan-treated mice (Extended Data Fig. 3h,i). The enhancement of interleukin-10 (IL-10) production was the result of an increase in Il10-expressing neutrophils (Fig. 3l–n), as there was no difference in IL-10 production in other cell types (Extended Data Fig. 3j–m). Collectively, these data indicate that β -glucan increases the number of neutrophils in blood circulation and promotes the recruitment of neutrophils expressing IL-10 into the lung tissue, promoting resolution in IAV-induced inflammation.

β-Glucan promotes granulopoiesis in the BM via type I IFN

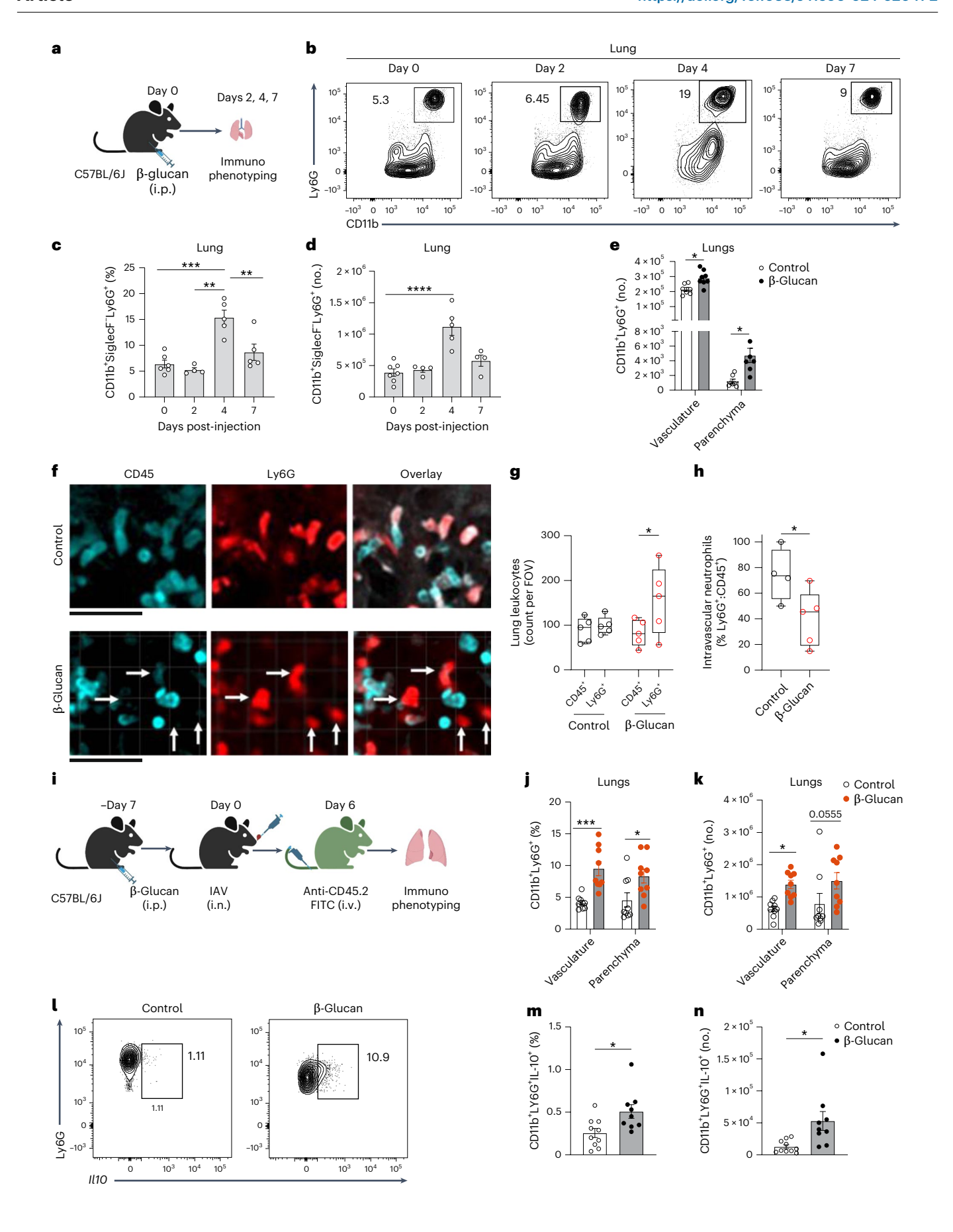
Recently, we demonstrated that two doses of β-glucan expand HSCs and promote myelopoiesis⁹. However, the increased number of neutrophils in the circulation of one dose of β-glucan treatment suggests that the β-glucan reprogramming of HSCs is biased toward granulopoiesis. Thus, we next investigated the effect of one dose of β -glucan on HSC expansion and the downstream progenitors (Extended Data Fig. 1b, gating strategy). Both the frequency and absolute number of LKS (Lin-cKit+Sca-1+), MPP (LKS+CD150-CD48+) and GMP (Lin-cKit+ CD34⁺CD16/32⁺) were significantly increased after β-glucan treatment (Fig. 4a-d and Extended Data Fig. 4a-c). GMP is upstream of common monocyte progenitors (cMoPs) or granulocyte progenitors (GPs) to generate neutrophils. It is interesting that we found increased GPs (Lin-Sca-1-cKit+CD16/32+CD34+CD115-Ly6c+) in the bone marrow (BM) with no differences in cMoPs (Lin-Sca-1-cKit+CD16/32+CD34+ CD115⁺Ly6c⁻), suggesting that one dose of β-glucan promotes granulopoiesis (Fig. 4e and Extended Data Fig. 4d,e) rather than myelopoiesis after two doses of β-glucan treatment. Increased GPs in the BM correlated with the increased frequency and absolute number of neutrophils in the BM (Fig. 4f-h). Next, we investigated the signaling pathway involved in the β-glucan reprogramming of HSCs toward granulopoiesis. β-Glucan primarily signals through the Dectin-1 receptor, which allows myeloid cells to sense invading fungal agents²³. We demonstrated that, in Dectin-1 deficient mice, the expansion of LKS cells and enhancement of granulopoiesis were lost after β-glucan treatment (Extended Data Fig. 4f-h). This indicates that Dectin-1 signaling is required for β-glucan-induced granulopoiesis. Moreover, two doses of β-glucan reprogramming of HSC/myelopoiesis depends on IL-1 signaling⁹. Thus, we next investigated whether IL-1 receptor (IL-1R) signaling is involved in regulating granulopoiesis after one dose of β-glucan. After one-dose β-glucan treatment, the number of neutrophils in the BM, blood and lungs increased in $Il1r^{-/-}$ mice (Fig. 4i-l and Extended Data Fig. 4i,j). Although there was no survival difference between *Il1r*^{-/-} and wild-type (WT) mice after a lethal dose of IAV infection, the survival of β -glucan-treated $Il1r^{-/-}$ mice was also comparable to β-glucan-treated WT mice post-IAV infection (Fig. 4m). Unexpectedly, these data suggest that IL-1 signaling is not required for the one-dose β-glucan-mediated granulopoiesis or protection against IAV.

Type I IFN has been shown to promote anti-tumor solid immunity via switching the function of the tumor-associated neutrophils²⁴. Therefore, we next investigated the potential role of type I IFN signaling in β-glucan training of neutrophils. Immunophenotyping of β-glucan-treated *Ifnar1*^{-/-} mice showed expansion of LKSs, MPPs and GMPs but failed to show an increase in GPs (Extended Data Fig. 4k-n). Consequently, *Ifnar1*^{-/-} mice showed no increased neutrophils in the BM, blood and lungs in response to β-glucan (Fig. 5a-c and Extended Data Fig. 4o-r). As has been shown previously²⁵, pulmonary neutrophils are increased in *Ifnar1*^{-/-} mice; however, β-glucan administration did not alter neutrophil numbers (Fig. 5d,e) These data collectively indicate that β-glucan promotes the expansion of HSCs and GMPs independent of type I IFN signaling, but type I IFN signaling is required for driving the fate of GMPs toward GPs. Next, we infected *Ifnar1*^{-/-} mice with IAV 7 d post-β-glucan treatment. We found that the *Ifnar1*^{-/-} mice are equally susceptible and succumbed to death after IAV infection and this susceptibility was irrespective of β-glucan treatment (Fig. 5f,g). To determine the critical role of type I IFN signaling in the BM against IAV, we next generated chimeric mice by reconstituting the congenic CD45.1 mice with the BM from either CD45.2 WT or *Ifnar1*^{-/-} mice (Fig. 5h). After 12 weeks, 90-95% of the recipient mice were reconstituted with the donor BM cells (Extended Data Fig. 4s). Similar to Ifnar1^{-/-} mice, β-glucan-treated WT mice reconstituted with the BM of Ifnar1^{-/-} mice revealed no enhancement in morbidity or mortality (Fig. 5i,j). These results further implicate the critical role of type I IFN signaling in the hematopoietic compartment for β-glucan-mediated protection against IAV. We next investigated whether the induction of type I IFN alone is sufficient to promote granulopoiesis. We administered polyinosinic:polycytidylic acid (poly(I:C)) i.p., a known inducer of type I IFN²⁶, and found that the frequency and absolute number of neutrophils were not increased in the lungs (Extended Data Fig. 4t-v). In addition, poly(I:C)-treated mice did not show enhanced survival against IAV infection (Extended Data Fig. 4w-x). Overall, these findings indicate that the combined signaling of Dectin-1 and type IIFN are required for β-glucan-mediated granulopoiesis. However, the induction of type I IFN alone is not sufficient to replicate $\beta\text{-glucan-mediated},$ trained immunity against IAV infection.

T cells are required to recruit β-glucan-trained neutrophils

Fig. 3 | β-Glucan treatment increases the recruitment of neutrophils to the lungs. a–d, Mice were treated with β-glucan and immune cells were assessed in the lungs at several time points (a). Representative FACS plots (b), frequency (c) and total cell counts (d) of neutrophils in the lungs are measured at days 2, 4 and 7 post-β-glucan treatment (n = 4–6). **e**, Intravascular staining at day 4 post-β-glucan treatment: total cell count of neutrophils in the vasculature and parenchyma of lungs (n = 5). **f**, Representative lung confocal intravital microscopy images comparing Ly6G-TdTom mice receiving saline i.p. versus mice treated with β-glucan i.p. Intravenous, fluorescently conjugated, anti-CD45 monoclonal antibody was used to mark intravascular leukocytes. Arrows highlight examples of Ly6G*CD45° cells. Scale bars, 50 μm. **g**, Visualized cells from the lung intravital images quantified by expression of either CD45 or Ly6G from control or β-glucan-treated mice. The horizontal lines represent the median, the bounds of the boxes indicate the 25th and 75th percentiles and the

whiskers represent the minima and maxima. Each dot representing an individual sample (n=5). **h**, The percentage of intravascular neutrophils in lung imaging was quantified as $Ly6G^*CD45^*/total\ Ly6G^*$ (n=5). **i**, Intravasculature staining at day 6 post-IAV infection. **j**, **k**, Frequency (**j**) and total cell counts (**k**) of neutrophils in the vasculature and parenchyma of lungs day 6 post-IAV infection (n=5). **l**, $III0^{GFP}$ reporter mice infected with IAV at day 7 post- β -glucan. The lungs were collected 6 d post-IAV infection. Representative FACS plots show $II10^{GFP}$ -Ly6G $^+$ cells as a percentage of Ly6G $^+$ cells. **m,n**, Frequency (**m**) and total cell counts (**n**) of II10-expressing neutrophils (n=5), data pooled from two individual experiments). Data are represented as mean \pm s.e.m. Data were analyzed using unpaired, two-tailed Student's t-test (**m** and **n**), one-way ANOVA followed by Tukey's multiple-comparison test (**c** and **d**) or two-way ANOVA followed by Šidák's multiple-comparison test (**e**, **g**, **h**, **j** and **k**). 'P<0.05, "P<0.01, "P<0.001, "P<0.0001. FOV, field of view. Illustrations in **a** and **i** created using BioRender.com.



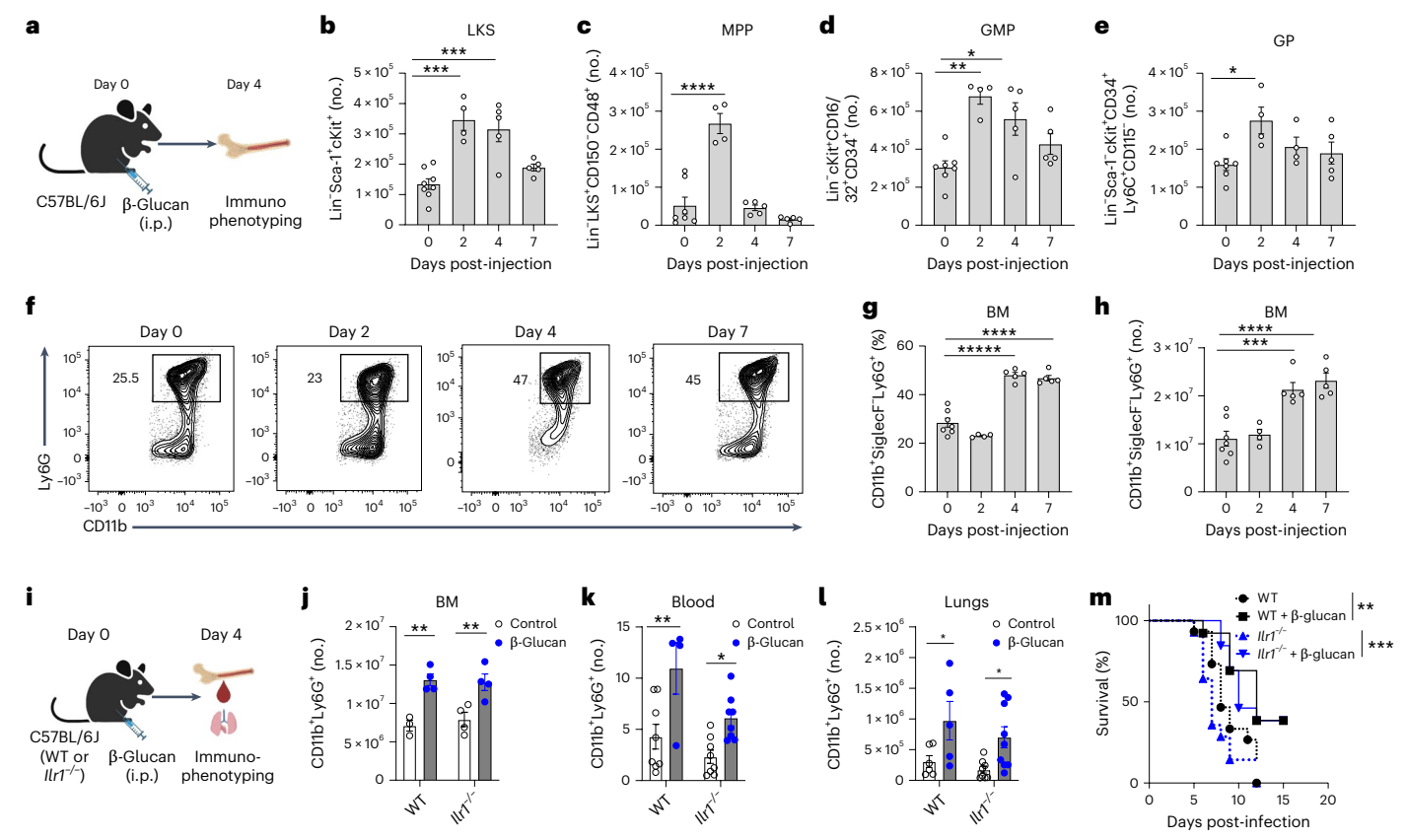


Fig. 4 | β-Glucan increases granulopoiesis and is independent of IL-1 signaling. a, Mice were treated with β-glucan, HSCs or progenitors and immune cells were assessed in the BM at days 2, 4 and 7 post-β-glucan treatment. **b**–**e**, Expansion of LKSs (**b**), MPPs (**c**), GMPs (**d**) and GPs (**e**) in the BM (n = 5). **f**–**h**, Representative FACS plots (**f**), frequency (**g**) and total cell counts of neutrophils (**h**) in the BM (n = 5). **i**, C57BL/6 (WT and $ll1r^{-/-}$) mice were treated with β-glucan. **j**–**l**, Neutrophils in the BM (**j**), blood (**k**) and lungs (**l**) at day 4 post-β-glucan

treatment (n=5). Data are pooled from two individual experiments. \mathbf{m} , Survival of $IIIr^{-/-}$ or WT mice after β -glucan treatment following IAV infection (lethal dose) at day 7 (n=10). Data are represented as mean \pm s.e.m. Data were analyzed using one-way ANOVA followed by Tukey's multiple-comparison test ($\mathbf{b}-\mathbf{e},\mathbf{g}$ and \mathbf{h}) or two-way ANOVA followed by Šidák's multiple-comparison tests ($\mathbf{j}-\mathbf{l}$). Survival was monitored by a log(rank) test (\mathbf{m}). P<0.05, P<0.01, P<0.001, P<0.001. Illustrations in \mathbf{a} and \mathbf{i} created using BioRender.com.

of the neutrophils into the lung, spleen and peritoneum was impaired in β -glucan-treated $Rag1^{-/-}$ mice (Fig. 6j and Extended Data Fig. 5b–f). Similarly, β -glucan-treated $Rag1^{-/-}$ mice failed to show an increase in the recruitment of neutrophils to the lungs post-IAV infection (Fig. 6k,l and Extended Data Fig. 5g,h). These data suggest that β -glucan promotes granulopoiesis independent of adaptive immunity, but adaptive immune cells are required to recruit neutrophils into the lung tissue.

Using multiplexed immunohistochemistry, we found increased neutrophil numbers, which were in proximity to CD4⁺ T cells and also increased in the lung parenchyma of WT β-glucan-treated mice (Fig. 6m,n). We then found that this increase of CD4⁺ T cells was partially caused by enhanced numbers of Roryt cells, in particular Roryt CD4⁺ T cells at day 4 post-β-glucan treatment (Fig. 60 and Extended Data Fig. 5i). The RoRy locus encodes a transcription factor required to differentiate IL-17-producing cells²⁷. IL-17A and IL-17F, ligands for IL-17 receptor (IL-17R), have been shown to mediate neutrophil migration into the lung in response to lippopolysaccharide or Gram-negative bacterial pneumonia^{28,29}. Defects in the IL-17 axis result in decreased neutrophil response associated with higher bacterial burden and poor survival of mice³⁰. Thus, we treated RoRyt^{GFP/GFP} mice (lacking expression of RoRγt) with β-glucan and found that, similar to WT mice, the frequency and total cell number of neutrophils were increased in the BM, suggesting that the increase of GPs in response to β-glucan was independent of Roryt⁺ T cells (Extended Data Fig. 5j). However, RoRyt^{GFP/GFP} mice failed to recruit neutrophils into the lung tissue after receiving β-glucan (Fig. 6p-r) 4 d post-treatment and after IAV

infection (Extended Data Fig. 5k–o). Furthermore, β -glucan-treated RoR γ t^{GFP/GFP} mice failed to show enhanced survival against IAV infection (Fig. 6s). Collectively, these data suggest that β -glucan treatment promotes granulopoiesis independent of adaptive immunity in the BM, but RoR γ T cells are required for the recruitment of neutrophils into the lung tissue.

β-Glucan reprograms neutrophils to a regulatory phenotype

Given that we observed distinct changes in levels of granulocyte progenitors in the BM after β -glucan, we next investigated whether recruited neutrophils in the lungs of β-glucan-treated mice showed differential imprinting. As neutrophils are short-lived and typically difficult to isolate, we performed single-cell RNA sequencing (scRNA-seq) on the lungs of mice at baseline, day 4 and day 7 post-β-glucan administration, focusing our analyses on the neutrophils. We captured a total of 925 high-quality neutrophil transcriptomes across treatment and control groups (Fig. 7a). At day 4 post-β-glucan, the peak of neutrophil expansion, we identified 194 differentially expressed genes (DEGs; false discovery rate (FDR) < 0.05) compared with controls (Fig. 7a-c). Gene-set enrichment analysis (GSEA) revealed that upregulated pathways were involved in the response to type IIFN, response to virus and regulation of innate immune response (Fig. 7d). By day 7, the number of DEGs in neutrophils decreased to 90 compared with controls, with only 16 upregulated genes (Fig. 7a-c). These genes included IFN-response genes (Ifitm3 and Oasl2) associated with viral control of IAV31-33 and neutrophil activation-related genes (Lrg1, Wfdc17 and Ctss)³⁴⁻³⁷.

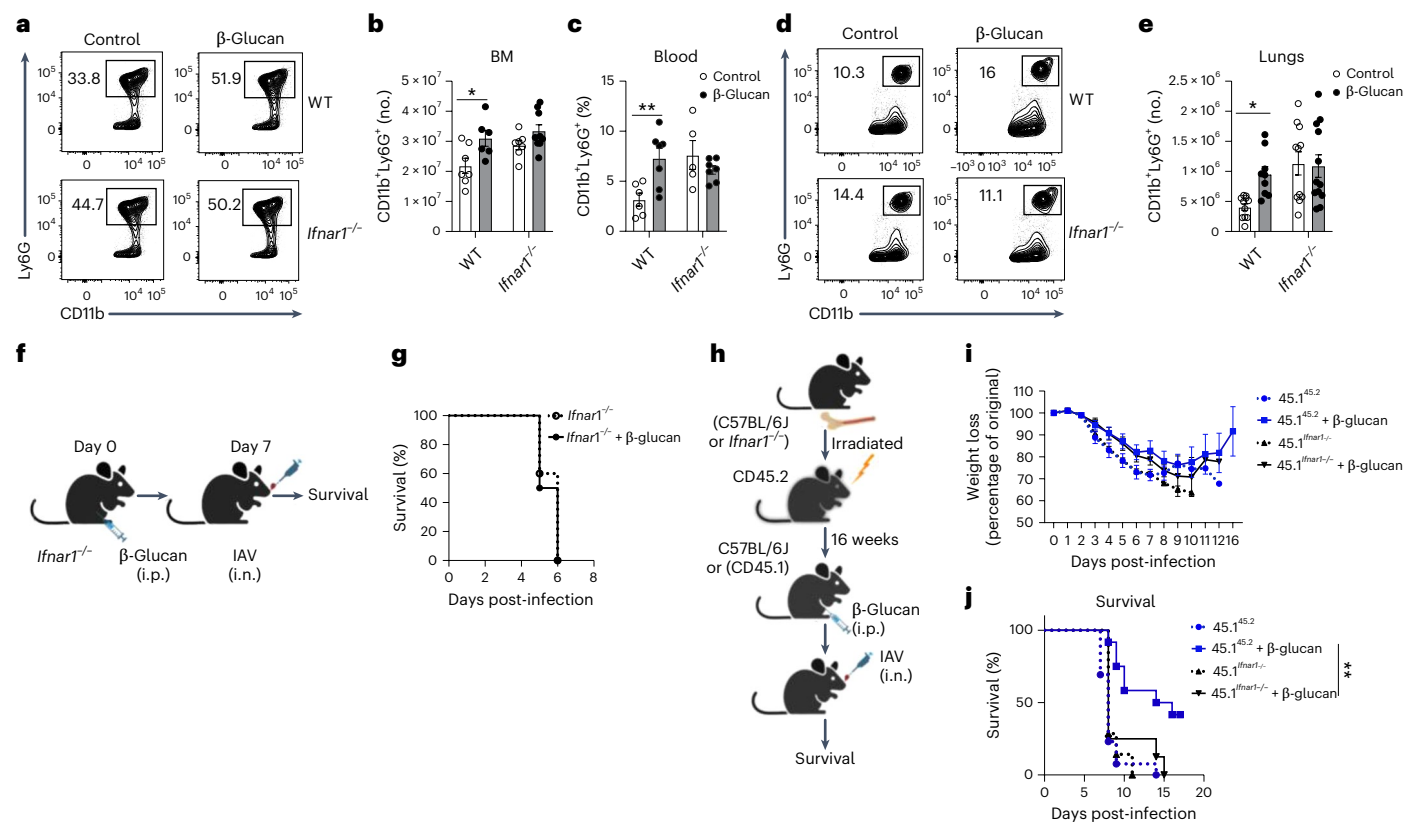


Fig. 5 | **β**-Glucan-mediated granulopoiesis requires type I IFN signaling. WT and $Ifnar1^{-/-}$ mice were treated with β-glucan. **a,b**, Representative FACS plots (**a**) and total cell counts (**b**) of neutrophils in the BM. **c**, Frequency of neutrophils in the blood (n = 5). **d,e**, Representative FACS plots (**d**) and total cell counts of neutrophils (**e**) in the lungs at day 4 post-β-glucan treatment (n = 8). **f,g**, Survival of C57BL/6 WT (**f**) or $Ifnar1^{-/-}$ (**g**) mice after β-glucan treatment following IAV infection (lethal dose) at day 7. **h**, Mouse chimera model. **i,i**, Weight loss (**i**) and

survival (**j**) of CD45.1 chimeric mice reconstituted with $IfnarI^{-/-}$ (CD45.2) BM after β -glucan treatment following IAV infection (lethal dose) on day 7 (n = 10). Data are represented as mean \pm s.e.m. Data were analyzed using two-way ANOVA followed by Šidák's multiple-comparison tests (**b**, **c**, **e** and **i**). Survival was monitored by a log(rank) test (**g** and **j**). P < 0.05, P < 0.01, P < 0.001, P < 0.0001. Illustrations in **f** and **h** created using BioRender.com.

Notably, neutrophils from β -glucan-treated mice showed enrichment of genes associated with antigen presentation (*H2-K1*, *Asprv1*, *Tap1* and *Cd74*), linked to a more regulatory function of neutrophils^{38–42}, as well as genes indicative of an immature phenotype (*Il1r2*, *Tspo*, *Plac8* and *H2-D1*)^{43–46}. This was consistent with surface protein expression quantified by MACSima segmentation, which showed enhanced expression of major histocompatibility complex (MHC) class II and reduced expression of Ly6G and CXCR4 on neutrophils (Extended Data Fig. 6a).

Neutrophils have long been considered to be terminally differentiated, homogeneous effector cells. In line with our findings, recent studies have demonstrated that neutrophils show a spectrum of plasticity from antimicrobial and proinflammatory to promote tissue healing and regulate inflammation⁴⁷. In fact, immature and mature neutrophils have been documented to differ not only in their surface marker expression but also in their functions⁴⁸. Therefore, to further investigate whether β-glucan reprogramming of HSCs gives rise to a unique subset of neutrophils, we employed multi-parameter spectral flow cytometry. We observed that β-glucan reprogramming led to a robust rearrangement of neutrophil clustering (Fig. 7e,f and Extended Data Fig. 6b,c). Using neutrophils isolated from the blood we showed that, under basal conditions, β-glucan shifted the whole neutrophil population toward a less activated phenotype (CD62Lhigh, CD11blow, CD49dlow) (Extended Data Fig. 6d,e), with lower levels of Ly6G, CXCR2 and CD101, suggesting a lower maturation stage. Strikingly, this reshaping appeared to be conserved under influenza infection, with β-glucan remaining the main driver of neutrophil clustering (Extended Data Fig. 6b,c). These data suggest that, even under inflammatory

conditions, β-glucan reprogramming was maintained in circulating neutrophils. Next, we investigated the impact of β-glucan reprogramming of neutrophils within IAV-infected lungs (Fig. 7e-h). Under IAV infection, neutrophils infiltrated the parenchyma of the lungs and, as expected, we could identify an IAV-driven population of neutrophils (Fig. 7e.f) which represented up to a third of the pulmonary pool (Fig. 7g). Despite the increased neutrophil infiltration after β-glucan treatment, we observed that trained neutrophils were less prone to give rise to IAV-driven clusters (Fig. 7f,g), which are kept <15% of the global lung populations in the infected lungs. As such, pulmonary neutrophil populations from β-glucan-treated mice maintained a less activated phenotype (CD62L^{high}, CD11b^{low}, CD49d^{low}) and appeared less mature (CD101^{low}, Ly6G^{low}, CD14^{low}) during IAV infection conditions (Fig. 7h). All together, these phenotypical data show that β-glucan reprogramming gives rise to a qualitative shift in neutrophil populations, which alters their behavior within the lungs after IAV infection. We further corroborated this by quantifying the kinetics of immature neutrophils (CD11b^{low}, Ly6G^{low}, CXCR2⁻) after IAV infection and demonstrated that β-glucan-treated mice had increased recruitment of immature neutrophils after IAV infection (Extended Data Fig. 6f,g). This suggests that this distinct neutrophil phenotype after β-glucan may contribute to the enhanced survival of treated mice against IAV infection.

Cellular metabolism plays an important role in the function and plasticity of diverse immune cells and the mechanism involved in metabolic regulations of neutrophils is continually unfolding. Interestingly, gene expression analyses revealed several metabolic pathways (for example, lipid and carbohydrate metabolism) that were significantly

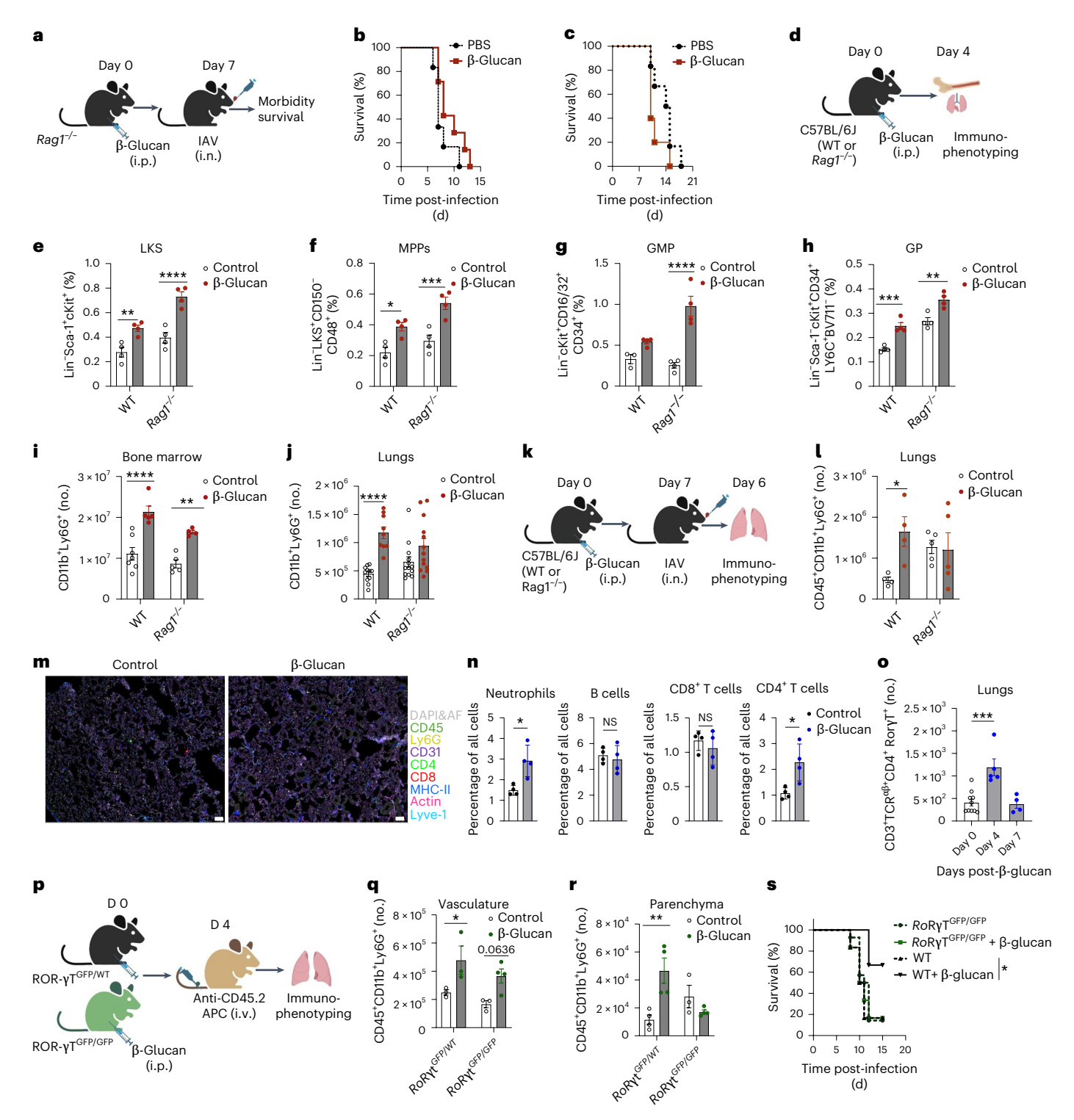


Fig. 6 | T cells are required for the recruitment of β-glucan-trained neutrophils to the lung tissue. \mathbf{a} - \mathbf{c} , $Rag \Gamma^{\leftarrow}$ mice (a) were infected with IAV lethal dose (b) and sublethal dose (c) at day 7 post-β-glucan treatment to assess survival (n=10). \mathbf{d} , C57BL/6 (WT and $Rag \Gamma^{\leftarrow}$) mice were treated with β-glucan. \mathbf{e} - \mathbf{h} , Expansion of LKSs (e), MPPs (f), GMPs (g) and GPs (h) assessed in the BM on day 4 post-β-glucan treatment (n=5). \mathbf{i} , Total cell counts of neutrophils in BM (i) and lungs (j) on day 4 post-β-glucan treatment (n=8). \mathbf{k} , C57BL/6 (WT and $Rag \Gamma^{\leftarrow}$) mice infected with IAV infection on day 7 post-β-glucan. I, Total cell counts of neutrophils in the lungs at day 6 post-IAV infection (n=4). \mathbf{m} , Mice were treated with β-glucan and after 4 d lungs subjected to MACSima imaging. \mathbf{n} , Quantification of corresponding pulmonary immune cells from MACSima

imaging (n = 4). **o**, Quantification of RORγt CD4* T cells after β-glucan treatment (n = 5). **p**, Intravascular staining of RORγt CD4* T cells after β-glucan treatment (n = 5). **p**, Intravascular staining of RORγt CD4* T cells in the lung vasculature β -glucan treatment. **q**, **r**, Total cell counts of neutrophils in the lung vasculature (**q**) and parenchyma (**r**) (n = 4). **s**, RORγt CGFP/GFP or RORγt WT/GFP mice infected with IAV (lethal dose) at day 7 post- β -glucan treatment to assess survival. Data are represented as mean \pm s.e.m. Data were analyzed using two-tailed, unpaired Student's t-test (**n**), one-way ANOVA followed by Tukey's multiple-comparison test (**o**) and two-way ANOVA followed by Šidák's multiple-comparison tests (**e**-**j**, **l**, **q** and **r**). Survival was monitored by a log(rank) test (**b**, **c** and **s**). P<0.005, P<0.001, P<0.001, P<0.0001. NS, not significant. Illustrations in **a**, **d**, **k** and **p** created using BioRender.com.

differentiated (FDR < 0.01) in their response to IAV infection when comparing nontreated with β -glucan-treated mice (Extended Data Fig. 6h,i). Thus, we further investigated the potential role of metabolic changes on the functional properties of β -glucan-reprogrammed neutrophils. Under basal conditions, neutrophils are glycolytic with very few mitochondria and thus, usually, mitochondria do not contribute significantly to their metabolism^{49,50}. However, neutrophils purified from β -glucan-treated mice rely on oxidative metabolism (Fig. 7i-m). An increase in mitochondrial respiration in \(\beta \)-glucan-reprogrammed neutrophils correlated with an increase in mitochondrial mass (Fig. 7n,o). To directly investigate the presence of β-glucan-trained neutrophils with increased mitochondria, Ly6G-TdTom mice were treated with either saline or β-glucan and lung intravital microscopy was performed. Mitotracker was administered intravenously (i.v.) to detect neutrophils with increased mitochondria. Similar to in vitro results, \(\beta \)-glucan-treated mice demonstrated significantly increased numbers of Mitotracker neutrophils in the lungs (Fig. 7p,q). These results showed that β-glucan generates a subset of regulatory neutrophils with unique transcriptional and metabolic programming, which differed from mature neutrophils. The increase of mitochondrial mass and oxygen consumption rate (OCR) in β-glucan-treated neutrophils was also dependent on type I IFN signaling, highlighting the critical role of type I IFN in reprogramming HSCs in the BM (Extended Data Fig. 6j-m).

Survival against IAV requires β -glucan-mediated neutrophils

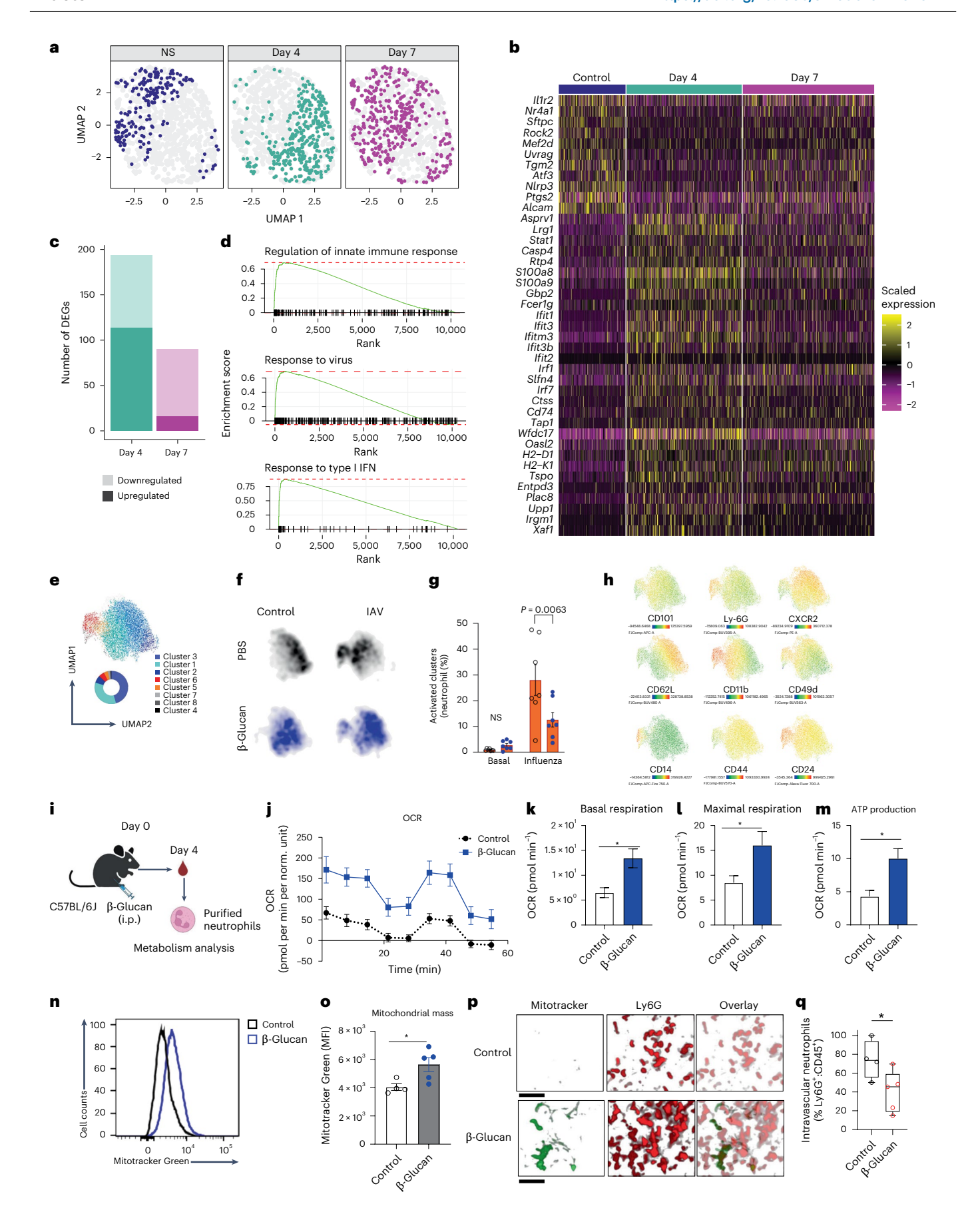
To directly assess the role of neutrophils in survival against IAV, we depleted neutrophils (anti-Ly6G) in control and β-glucan-treated mice starting 1 d before the IAV infection and continued up to 7 d consecutively (Fig. 8a). Depletion of neutrophils was confirmed (Extended Data Fig. 7a,b) which abrogated the survival advantage of β-glucan-treated mice after IAV infection. This demonstrates that β-glucan-trained neutrophils were essential for host survival after a lethal infection with IAV (Fig. 8b,c). To further investigate whether this enhanced survival against IAV was mediated by β-glucan-trained neutrophils and not monocytes, we performed a series of experiments using Ccr2^{-/-} mice that possess monocytes that cannot egress from the BM. Similar to WT mice, treatment of $Ccr2^{-/-}$ mice with β -glucan led to an increase in neutrophils in the BM, blood and lungs on day 4 post-β-glucan treatment (Extended Data Fig. 7c-g), Importantly, $Ccr2^{-/-}$ mice receiving β -glucan showed reduced weight loss and enhanced survival against IAV infection (Extended Data Fig. 7h-j). Thus, β-glucan increased host survival against IAV infection independent of monocytes. To corroborate the loss-of-function with gain-of-function experiments, we performed an intravenous adoptive transfer of purified neutrophils isolated from the BM of either control or β-glucan-treated mice into naive recipient mice (Fig. 8d). We first confirmed the recruitment of transferred neutrophils into the lungs of recipient mice by flow cytometry (Extended Data Fig. 7k). Importantly, the adoptive transfer of neutrophils from β-glucan-treated mice conferred a survival advantage compared with the mice that received control neutrophils or no transfer controls (Fig. 8e,f). These findings indicate that β-glucan-trained neutrophils alone can enhance the survival of mice during IAV infection. Finally, we used IFNAR^{flox} × Mrp8^{Cre} mice, which lack type I IFN signaling mainly in the granulocyte progenitors (GMPs). After β-glucan administration, IFNAR^{flox} × Mrp8^{Cre} mice showed an expansion of LKS⁺ cells, but not GMPs or GPs, confirming the requirement of type I IFN for promoting granulopoiesis after β-glucan (Extended Data Fig. 7l-r). As type I IFN signaling is required for reprogramming of neutrophils by β-glucan, IFNAR^{flox} × Mrp8^{Cre} mice treated with β-glucan did not exhibit a survival advantage after a lethal infection of IAV (Fig. 8g-i). Collectively, these findings indicate β-glucan-mediated host survival against IAV infection via reprogramming neutrophils in type I IFN-dependent manner.

Discussion

Although severe pneumonia in most patients on the intensive care unit is caused by impaired disease tolerance^{51,52}, the cellular and molecular mechanisms underlying this process remain poorly understood. Our limited understanding of immunity against infectious diseases may partly stem from a bias toward studying host resistance. Aberrant pulmonary innate immune responses correlate with the pathogenesis of multiple human respiratory viral infections, including IAV infection⁴. Although proinflammatory cytokine or chemokine production by innate immune cells (for example, macrophages) and innate immune cell recruitment are required for host resistance to pulmonary viral infections, cytokine dysregulation is associated with a 'cytokine storm', which exacerbates lung injury and has poor clinical outcomes⁵³. Thus, a controlled innate immune response to pulmonary viral infections is essential for preventing excessive lung tissue pathology and preserving lung function. In the present study, we have demonstrated that \(\beta\)-glucan enhanced host survival against lethal IAV infection via reprogramming of HSCs toward granulopoiesis, generating a unique subset of regulatory neutrophils, which were required to promote disease tolerance against IAV infection. The immunomodulatory activity of β-glucan depends on its physical properties⁵⁴. Among the various structural conformations of β -glucan linkages, including $\beta(1,3)$, $\beta(1,4)$ and $\beta(1.6)$, only molecules with a $\beta(1.3)$ -linked D-glucose backbone has been shown to be immunomodulatory²⁰. We also found that the strength of β-glucan signaling has a profound impact on the outcome of innate memory responses. In the present study, we demonstrated that one-dose of β-glucan administration promotes granulopoiesis and neutrophil differentiation, with no significant difference in the

Fig. 7 B-Glucan training induces robust changes in neutrophils phenotype and metabolism. a, UMAP of 925 lung neutrophils isolated from nontreated mice and mice challenged with β-glucan for 4 and 7 d. b, Heatmap of scaled expression levels of select DEGs (FDR < 0.05) at day 4 post β -glucan treatment. c, Number of DEGs 4 and 7 d after β -glucan treatment. **d**, Enrichment plots of representative upregulated (FDR < 0.05) GO pathways 4 d after β-glucan treatment. e-h, Mice were treated with β-glucan 6 d before influenza infection. On day 9 post-β-glucan treatment, lung neutrophils from infected and noninfected mice were extracted and their surface phenotype was assessed by spectral flow cytometry. e, UMAP of CD11b⁺Lv6G⁺ neutrophils with and without influenza infection. Neutrophils separate in eight Flowsom Clusters. f, UMAP from b projected for the four experimental groups (PBS \pm influenza, black and β -glucan \pm influenza, dark blue). Clusters 5, 6 and 8 expand dramatically during influenza infection. g, Quantification of neutrophil present in influenza-driven clusters (clusters 5, 6 and 8). h, Mean fluorescence intensity (MFI) of selected markers projected on the UMAP from **f**. Influenza-driven clusters exhibit an activated phenotype (CD14high, CD24high CD11bhigh, CD62Llow, CD49dlow). UMAPs are based on 16 surface markers: CD45, Ly6G, CD101, CXCR2, CXCR4, CD62L, CD24, CD11b,

CD49d, CD44, CCR2, Lv6C, CD80, MHC-II, CD16, CD14 (n = 7), i, Mice were treated with β-glucan. Neutrophils were purified from blood on day 4 post- $\beta d\text{-glucan treatment.}\textbf{\textit{j}}\textbf{-}\textbf{\textit{m}}, Neutrophils' cellular metabolism determined by$ Seahorse (j), basal respiration (k), maximal respiration (l) and ATP production (m). n,o, Representative histogram plot (n) and quantification (MFI) (o) for mitochondrial mass using Mitotracker Green dye in the neutrophils of β -glucantreated mice (n = 4). **p**, Representative three-dimensional reconstructed lung intravital microscopy images from control or β -glucan-treated Ly6G-TdTom mice. Mitotracker Green dye was given i.v. before imaging. Scale bars, $50~\mu m$. \mathbf{q} , Mitochondria bright neutrophils quantified (n = 4). The horizontal lines represent the median, the bounds of the boxes indicate the 25th and 75th percentiles and the whiskers represent the minima and maxima. Each dot represents an individual sample (n = 4). Data are represented as mean \pm s.e.m. Data were analyzed using two-way ANOVA followed by Šidák's multiplecomparison tests (\mathbf{j}) and two-tailed, unpaired Student's t-test (\mathbf{k} - \mathbf{m} , \mathbf{o} and \mathbf{q}). *P<0.05, "P<0.01, ""P<0.001. Norm., normalized. Illustration in i created using BioRender.com.



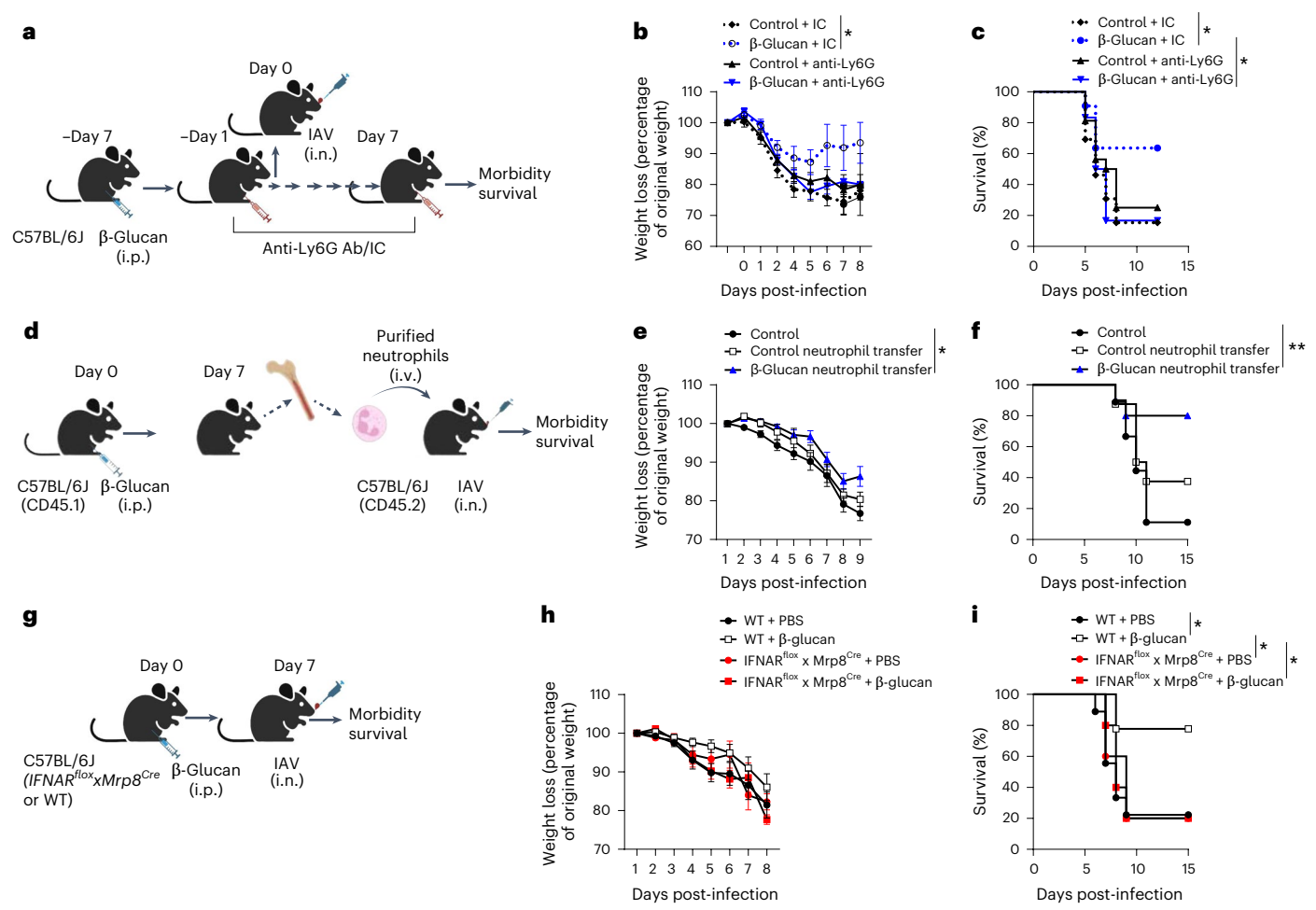


Fig. 8 | β-Glucan-driven protection against IAV is dependent on trained neutrophils. a, Schematic of neutrophil depletion experiment using anti-Ly6G antibodies. Mice were infected with IAV (lethal dose) at day 7 post-β-glucan treatment. Anti-Ly6G antibody or isotype control (IC) was administered (i.p.) on day 1 before infection and daily until day 7. b,c, Weight loss (b) and survival (c) monitored over time (n = 10). d, Schematic of adoptive transfer experiment. Neutrophils were isolated from CD45.1 control or β-glucan donor mice and adoptively transferred into naive CD45.2 recipient mice, which were infected

with a lethal dose of IAV. **e**, **f**, Weight loss (**e**) and survival (**f**) monitored over time (n = 10). **g**, IFNAR^{flox} × Mrp8^{Cre} mice were infected with IAV (lethal dose) at day 7 post- β -glucan. **h**, **i**, Weight loss (**h**) and survival (**i**) monitored over time (n = 8). Data are represented as mean \pm s.e.m. Data were analyzed using two-way ANOVA followed by Šidák's multiple-comparison tests (**b**, **e** and **h**). Survival was monitored by a log(rank) test (**c**, **f** and **i**). P < 0.05, P < 0.01. Illustrations in **a**, **d**, **g** created using BioRender.com.

myelopoiesis or monocytopoiesis that we have previously observed with two doses of β -glucan against Mtb^9 .

Importantly, the signaling pathway involved in β -glucan-mediated granulopoiesis was dependent on type HFN, wheres β-glucan-mediated myelopoiesis required IL-1β signaling^{9,11}. After one-dose β-glucan administration, Mitroulis and colleagues observed increased MPPs in the BM dependent on IL-1β signaling⁵⁵. This is consistent with our observation that β-glucan treatment increased the LKS, MPP and GMP population. However, the production of GPs, which are downstream of GMPs, was dependent on type 1 IFN signaling. Ifnar1-/- mice showed expansion of LKSs, MPPs and GMPs in response to β-glucan treatment but with no increase in the GP population downstream of GMPs. Similarly, a recently published study shows that granulopoiesis in the BM after one-dose β-glucan treatment in the setting of cancer depends on the type I IFN pathway¹¹. In addition, Dectin-1 recognizes β-glucan and we found that Dectin-1 signaling is required for induction of granulopoiesis after one-dose β -glucan. However, further investigation is needed to elucidate the differential impact of one versus two doses of β-glucan on HSCs. The strength of the β-glucan immunomodulatory effects may be cumulative or repeated doses may induce attenuation or tolerance of the initial signal. Nevertheless, the HSC compartment is a highly protected niche of our immune system, therefore even slight perturbations within these populations can yield a wide range of downstream effects. B-Glucan has long been established as influencing the mobilization of HSCs⁵⁶, with the recently trained immunity studies revealing the breadth of impact that this agent can have on the entire $system \ensuremath{^{9.55,57,58}}. As poly (I:C) alone failed to reprogram granulopoies is and$ generate trained neutrophils, we hypothesized that β-glucan-mediated granulopoiesis requires two signals: (1) Dectin-1 and (2) type I IFN signaling. In addition, we speculated that the HSC response is context dependent. For instance, in the context of IAV infection, type I IFN was a major driver in the generation of trained GMPs or neutrophils, whereas in Mtb infection IL-1 signaling was dominant. It can be postulated that the nature of the infectious agent and ensuing inflammatory microenvironment contributes to which signaling pathways are beneficial in HSC reprogramming, with IAV causing an acute viral infection and Mtb a chronic bacterial infection. The presence of pathogens, pathogen products and host mediators (for example, cytokines) provides a complex matrix and how HSCs perceive and/or respond to these signals requires further investigations^{59,60}.

Although the reprogramming of HSCs/GMPs/GPs/neutrophils was entirely independent of adaptive immune cells, the recruitment

of trained neutrophils into the lung required T cells. Our findings are in line with the evidence that T lymphocytes are involved in orchestrating the sustained mobilization of neutrophils⁶¹. Although we did not investigate the cytokine(s) involved in neutrophil recruitment into the lung, we identified that Roryt cells were required for this recruitment. Helper 17 T cells (T_H17 cells), γδ T cells and type 3 innate lymphoid cells express Roryt and can produce IL-17, which is essential for neutrophil recruitment into the lungs and protection against pathogens⁶². Moreover, the susceptibility of the β-glucan-treated T and B cell-deficient host to IAV infection is an indication of the important crosstalk between trained and adaptive immunity. We have also recently demonstrated how Bacillus Calmette-Guérin (BCG) vaccination provides cross-protection against IAV infection via a dialog between conventional effector memory T cells and innate memory cells⁶³. This highlights how both arms of innate and adaptive memory responses are required for coordinating an optimal host defense against pulmonary infections.

Neutrophils were conventionally considered a homogeneous, short-lived population, highly inflammatory and enhancing host resistance against mainly bacterial and fungal infections⁶⁴. However, recent studies revealed that neutrophils are heterogeneous, exhibiting functions ranging from inflammatory to anti-inflammatory and pro-healing. During viral infections, neutrophils are recruited to infection sites but are less directly involved in virus elimination. Our findings add to growing evidence demonstrating neutrophils' regulatory role in controlling inflammation and promoting tissue regeneration and healing after injury. Treatment with β-glucan reprogrammed the BM HSCs to generate a unique subset of neutrophils with a regulatory phenotype. Our transcriptomic data also suggest this subset of neutrophils may act as antigen-presenting cells (APCs) which have been shown to play a regulatory role via crosstalk with lymphocytes and attenuation of inflammatory immune cells^{65–67}. Furthermore, metabolic adaptation of neutrophils has been identified as the critical component in defining neutrophils' functions. Neutrophils are typically considered to be oligomitochondrial cells and their mitochondria associated with cell-death programs⁶⁸. However, unlike mature neutrophils, which preferentially utilize glycolysis for energetics, immature neutrophils rely on mitochondrial respiration for energy production. It has been shown that the tumor microenvironment induces metabolic adaptation in neutrophils with increased mitochondrial fitness and immunosuppression⁶⁹. We also found that β-glucan reprogrammed HSCs to generate regulatory neutrophils with a distinct transcriptional program to maintain and utilize mitochondrial respiration for their energy demands. Although we show that a potential mechanism of β-glucan-induced neutrophils is enhanced IL-10 production, the exact cellular and molecular mechanism(s) of how these regulatory neutrophils control inflammation and/or promote lung tissue repair requires further investigation.

The longevity and capacity of memory innate immune cells across various contexts, including sterile inflammation, infections and cancer, remain poorly understood. Our previous work demonstrated that HSC reprogramming and protective immunity persist for at least a year after BCG vaccination 70 , whereas BCG's cross-protection against influenza lasts 6 months 63 . Similarly, Mitroulis et al. showed long-term HSC reprogramming by β -glucan using BM reconstitution 55 . In the present study, we observed β -glucan's protective effects lasting up to 30 d, although the persistence of this protective signature warrants further investigation.

Finally, most studies on innate memory responses have been focused on the proinflammatory behavior of innate immune cells and their contributions to host resistance; little is known about their potential in regulating inflammation and promoting disease tolerance. Considering the limited therapeutic options available for severe pulmonary viral infections, promoting disease tolerance via innate memory responses may be a feasible translational approach.

Online content

Any methods, additional references, Nature Portfolio reporting summaries, source data, extended data, supplementary information, acknowledgements, peer review information; details of author contributions and competing interests; and statements of data and code availability are available at https://doi.org/10.1038/s41590-024-02041-2.

References

- Medzhitov, R., Schneider, D. S. & Soares, M. P. Disease tolerance as a defense strategy. Science 335, 936–941 (2012).
- Meunier, I., Kaufmann, E., Downey, J. & Divangahi, M. Unravelling the networks dictating host resistance versus tolerance during pulmonary infections. *Cell Tissue Res.* 367, 525–536 (2017).
- 3. Divangahi, M. Are tolerance and training required to end TB? Nat. Rev. Immunol. **18**, 661–663 (2018).
- 4. Pernet, E., Downey, J., Vinh, D. C., Powell, W. S. & Divangahi, M. Leukotriene B_4 -type I interferon axis regulates macrophage-mediated disease tolerance to influenza infection. *Nat. Microbiol.* **4**, 1389–1400 (2019).
- Downey, J. et al. Mitochondrial cyclophilin D promotes disease tolerance by licensing NK cell development and IL-22 production against influenza virus. Cell Rep. 39, 110974 (2022).
- Divangahi, M. et al. Trained immunity, tolerance, priming and differentiation: distinct immunological processes. *Nat. Immunol.* 22, 2–6 (2021).
- Netea, M. G., Schlitzer, A., Placek, K., Joosten, L. A. B. & Schultze, J. L. Innate and adaptive immune memory: an evolutionary continuum in the host's response to pathogens. Cell Host Microbe 25, 13–26 (2019).
- 8. Kaufmann, E. et al. BCG educates hematopoietic stem cells to generate protective innate immunity against tuberculosis. *Cell* **172**, 176–190.e119 (2018).
- Moorlag, S. et al. β-Glucan induces protective trained Immunity against Mycobacterium tuberculosis Infection: a key role for IL-1. Cell Rep. 31, 107634 (2020).
- Geller, A. E. et al. The induction of peripheral trained immunity in the pancreas incites anti-tumor activity to control pancreatic cancer progression. *Nat. Commun.* 13, 759 (2022).
- Kalafati, L. et al. Innate immune training of granulopoiesis promotes anti-tumor activity. Cell 183, 771–785.e712 (2020).
- Gustine, J. N. & Jones, D. Immunopathology of hyperinflammation in COVID-19. Am. J. Pathol. 191, 4–17 (2021).
- Kruger, P. et al. Neutrophils: between host defence, immune modulation, and tissue injury. PLoS Pathog. 11, e1004651 (2015).
- Herrero-Cervera, A., Soehnlein, O. & Kenne, E. Neutrophils in chronic inflammatory diseases. *Cell Mol. Immunol.* 19, 177–191 (2022).
- Skokowa, J., Dale, D. C., Touw, I. P., Zeidler, C. & Welte, K. Severe congenital neutropenias. Nat. Rev. Dis. Prim. 3, 17032 (2017).
- Pernet, E. et al. Neonatal imprinting of alveolar macrophages via neutrophil-derived 12-HETE. Nature 614, 530–538 (2023).
- Wang, J. Neutrophils in tissue injury and repair. Cell Tissue Res. 371, 531–539 (2018).
- 18. Soehnlein, O. et al. Neutrophil-derived cathelicidin protects from neointimal hyperplasia. Sci. Transl. Med. 3, 103ra198 (2011).
- Ferraro, B. et al. Pro-angiogenic macrophage phenotype to promote myocardial repair. J. Am. Coll. Cardiol. 73, 2990–3002 (2019).
- 20. Batbayar, S., Lee, D. H. & Kim, H. W. Immunomodulation of fungal β -glucan in host defense signaling by Dectin-1. *Biomol. Ther.* **20**, 433–445 (2012).
- Ruscitti, C. et al. Recruited atypical Ly6G⁺ macrophages license alveolar regeneration after lung injury. Sci. Immunol. 9, eado1227 (2024).

- Niggli, V. Signaling to migration in neutrophils: importance of localized pathways. Int. J. Biochem. Cell Biol. 35, 1619–1638 (2003).
- Brown, G. D. et al. Dectin-1 mediates the biological effects of beta-glucans. J. Exp. Med. 197, 1119–1124 (2003).
- Pylaeva, E., Lang, S. & Jablonska, J. The essential role of type I interferons in differentiation and activation of tumor-associated neutrophils. Front. Immunol. 7, 629 (2016).
- 25. Wu, C. F. et al. The lack of type I interferon induces neutrophil-mediated pre-metastatic niche formation in the mouse lung. *Int J. Cancer* **137**, 837–847 (2015).
- Alexopoulou, L., Holt, A. C., Medzhitov, R. & Flavell, R. A. Recognition of double-stranded RNA and activation of NF-kappaB by Toll-like receptor 3. Nature 413, 732–738 (2001).
- 27. Zhang, H. et al. CD109 restrains activation of cutaneous IL-17-producing $\gamma\delta$ T cells by commensal microbiota. *Cell Rep.* **29**, 391–405.e395 (2019).
- 28. Crowe, C. R. et al. Critical role of IL-17RA in immunopathology of influenza infection. *J. Immunol.* **183**, 5301–5310 (2009).
- 29. Shibata, K., Yamada, H., Hara, H., Kishihara, K. & Yoshikai, Y. Resident Vdelta1+ gammadelta T cells control early infiltration of neutrophils after *Escherichia coli* infection via IL-17 production. *J. Immunol.* **178**, 4466–4472 (2007).
- Ye, P. et al. Requirement of interleukin 17 receptor signaling for lung CXC chemokine and granulocyte colony-stimulating factor expression, neutrophil recruitment, and host defense. *J. Exp. Med.* 194, 519–527 (2001).
- Poddar, S., Hyde, J. L., Gorman, M. J., Farzan, M. & Diamond, M. S. The interferon-stimulated gene IFITM3 restricts infection and pathogenesis of arthritogenic and encephalitic alphaviruses.
 J. Virol. 90, 8780–8794 (2016).
- Regino-Zamarripa, N. E. et al. Differential leukocyte expression of IFITM1 and IFITM3 in patients with severe pandemic influenza A(H1N1) and COVID-19. J. Interferon Cytokine Res. 42, 430–443 (2022).
- Ivan, F. X. et al. Neutrophils infected with highly virulent influenza H3N2 virus exhibit augmented early cell death and rapid induction of type I interferon signaling pathways. Genomics 101, 101–112 (2013).
- 34. Druhan, L. J. et al. Leucine rich α -2 glycoprotein: a novel neutrophil granule protein and modulator of myelopoiesis. *PLoS ONE* **12**, e0170261 (2017).
- Zhao, Y. et al. Thrombospondin-1 restrains neutrophil granule serine protease function and regulates the innate immune response during *Klebsiella pneumoniae* infection. *Mucosal Immunol.* 8, 896–905 (2015).
- Liu, X. H. et al. Single-cell RNA sequencing reveals a novel inhibitory effect of ApoA4 on NAFL mediated by liver-specific subsets of myeloid cells. Front. Immunol. 13, 1038401 (2022).
- McKelvey, M. C. et al. Cathepsin S contributes to lung inflammation in acute respiratory distress syndrome. *Am. J. Respir. Crit. Care Med.* 205, 769–782 (2022).
- 38. Li, Y. et al. The regulatory roles of neutrophils in adaptive immunity. *Cell Commun. Signal.* **17**, 147 (2019).
- Mysore, V. et al. FcγR engagement reprograms neutrophils into antigen cross-presenting cells that elicit acquired anti-tumor immunity. Nat. Commun. 12, 4791 (2021).
- Whittaker Hawkins, R. F. et al. ICAM1+ neutrophils promote chronic inflammation via ASPRV1 in B cell-dependent autoimmune encephalomyelitis. JCI Insight 2, e96882 (2017).
- Jin, H. et al. Antigen-presenting aged neutrophils induce CD4⁺ T cells to exacerbate inflammation in sepsis. J. Clin. Invest. 133, e164585 (2023).
- 42. Reyes, L. et al. A type I IFN, prothrombotic hyperinflammatory neutrophil signature is distinct for COVID-19 ARDS. *Wellcome Open Res.* **6**, 38 (2021).

- de Lima, C. B. et al. Actions of translocator protein ligands on neutrophil adhesion and motility induced by G-protein coupled receptor signaling. *Biochem. Biophys. Res. Commun.* 417, 918–923 (2012).
- 44. Montaldo, E. et al. Cellular and transcriptional dynamics of human neutrophils at steady state and upon stress. *Nat. Immunol.* **23**, 1470–1483 (2022).
- 45. Kwok, A. J. et al. Neutrophils and emergency granulopoiesis drive immune suppression and an extreme response endotype during sepsis. *Nat. Immunol.* **24**, 767–779 (2023).
- Grieshaber-Bouyer, R. et al. The neutrotime transcriptional signature defines a single continuum of neutrophils across biological compartments. *Nat. Commun.* 12, 2856 (2021).
- Peiseler, M. & Kubes, P. More friend than foe: the emerging role of neutrophils in tissue repair. J. Clin. Invest. 129, 2629–2639 (2019).
- 48. Rosales, C. Neutrophil: a cell with many roles in inflammation or several cell types? *Front. Physiol.* **9**, 113 (2018).
- Sadiku, P. et al. Neutrophils fuel effective immune responses through gluconeogenesis and glycogenesis. *Cell Metab.* 33, 1062–1064 (2021).
- 50. Jeon, J. H., Hong, C. W., Kim, E. Y. & Lee, J. M. Current understanding on the metabolism of neutrophils. *Immune Netw.* **20**, e46 (2020).
- 51. Brun-Buisson, C. The epidemiology of the systemic inflammatory response. *Intens. Care Med.* **26**, S64–S74 (2000).
- Xiao, W. et al. A genomic storm in critically injured humans.
 J. Exp. Med. 208, 2581–2590 (2011).
- 53. Perrone, L. A., Plowden, J. K., García-Sastre, A., Katz, J. M. & Tumpey, T. M. H5N1 and 1918 pandemic influenza virus infection results in early and excessive infiltration of macrophages and neutrophils in the lungs of mice. *PLoS Pathog.* **4**, e1000115 (2008).
- 54. Murphy, E. J., Rezoagli, E., Major, I., Rowan, N. J. & Laffey, J. G. β-Glucan metabolic and immunomodulatory properties and potential for clinical application. *J. Fungi* **6**, 356 (2020).
- Mitroulis, I. et al. Modulation of myelopoiesis progenitors Is an integral component of trainedimmunity. Cell 172, 147–161.e112 (2018).
- Patchen, M. L. et al. Mobilization of peripheral blood progenitor cells by Betafectin PGG-Glucan alone and in combination with granulocyte colony-stimulating factor. Stem Cells 16, 208–217 (1998).
- Stothers, C. L. et al. β-Glucan induces distinct and protective innate immune memory in differentiated macrophages.
 J. Immunol. 207, 2785–2798 (2021).
- Camilli, G., Tabouret, G. & Quintin, J. The complexity of fungal β-glucan in health and disease: effects on the mononuclear phagocyte system. Front. Immunol. 9, 673 (2018).
- Scumpia, P. O. et al. Cutting edge: bacterial infection induces hematopoietic stem and progenitor cell expansion in the absence of TLR signaling. J. Immunol. 184, 2247–2251 (2010).
- 60. Baldridge, M. T., King, K. Y. & Goodell, M. A. Inflammatory signals regulate hematopoietic stem cells. *Trends Immunol.* **32**, 57–65 (2011).
- 61. Liu, R. et al. IL-17 promotes neutrophil-mediated immunity by activating microvascular pericytes and not endothelium. *J. Immunol.* **197**, 2400–2408 (2016).
- 62. Borkner, L., Curham, L. M., Wilk, M. M., Moran, B. & Mills, K. H. G. IL-17 mediates protective immunity against nasal infection with *Bordetella pertussis* by mobilizing neutrophils, especially Siglec-F⁺ neutrophils. *Mucosal Immunol.* **14**, 1183–1202 (2021).
- Tran, K. A. et al. BCG immunization induces CX3CR1^{hi} effector memory T cells to provide cross-protection via IFN-γ-mediated trained immunity. *Nat. Immunol.* 25, 418–431 (2024).

- 64. Lehman, H. K. & Segal, B. H. The role of neutrophils in host defense and disease. J. Allergy Clin. Immunol. **145**, 1535–1544 (2020).
- Mantovani, A., Cassatella, M. A., Costantini, C. & Jaillon, S. Neutrophils in the activation and regulation of innate and adaptive immunity. *Nat. Rev. Immunol.* 11, 519–531 (2011).
- 66. Kalyan, S. & Kabelitz, D. When neutrophils meet T cells: beginnings of a tumultuous relationship with underappreciated potential. *Eur. J. Immunol.* **44**, 627–633 (2014).
- Barquero-Calvo, E. et al. Neutrophils exert a suppressive effect on Th1 responses to intracellular pathogen *Brucella abortus*. *PLoS Pathog*. 9, e1003167 (2013).
- 68. Maianski, N. A. et al. Functional characterization of mitochondria in neutrophils: a role restricted to apoptosis. *Cell Death Differ.* **11**, 143–153 (2004).
- Rogers, T. & DeBerardinis, R. J. Metabolic plasticity of neutrophils: relevance to pathogen responses and cancer. *Trends Cancer* 7, 700–713 (2021).
- Khan, N. et al. M. tuberculosis reprograms hematopoietic stem cells to limit myelopoiesis and impair trained immunity. Cell 183, 752–770.e722 (2020).

Publisher's note Springer Nature remains neutral with regard to jurisdictional claims in published maps and institutional affiliations.

Open Access This article is licensed under a Creative Commons Attribution-NonCommercial-NoDerivatives 4.0 International License, which permits any non-commercial use, sharing, distribution and reproduction in any medium or format, as long as you give appropriate credit to the original author(s) and the source, provide a link to the Creative Commons licence, and indicate if you modified the licensed material. You do not have permission under this licence to share adapted material derived from this article or parts of it. The images or other third party material in this article are included in the article's Creative Commons licence, unless indicated otherwise in a credit line to the material. If material is not included in the article's Creative Commons licence and your intended use is not permitted by statutory regulation or exceeds the permitted use, you will need to obtain permission directly from the copyright holder. To view a copy of this licence, visit http://creativecommons.org/licenses/by-nc-nd/4.0/.

© The Author(s) 2025, corrected publication 2025

Methods

Mice

Six- to ten-week-old C57BL/6, CD45.1, Ifnar1^{-/-}, IL-1R^{-/-}, Rag1^{-/-}, RoRγt^{GFP/GFP}, $Ccr2^{-/-}$, IFNAR^{flox}, B6.Cg-Tg(S100A8-cre) and VertX ($II10^{GFP}$) mice were purchased from Jackson Laboratories. All animal studies were conducted in accordance with the guidelines of, and approved by, the Animal Research Ethics Board of McGill University (project ID no. 5860). All animals were housed and inbred at the animal facility of the Research Institute of McGill University under specific pathogen-free conditions: access to food and water, temperature of 21 °C (\pm 1 °C), relative humidity of 40–60% (\pm 5%) and light cycle of 12 h ON:12 h OFF (daily cycle). Experiments were conducted using male and female sexand age-matched mice that were randomly assigned to experimental groups. Only female mice are used in experiments using IAV infection. No statistical methods were used to predetermine sample size but are similar to those reported in previous publications 63,70.

B-Glucan treatment

Mice were treated with β -glucan (Sigma-Aldrich, cat. no. G5011), 1 mg per mouse in 100 μ l of phosphate-buffered saline (PBS) i.p.

Viruses and infection

All in vivo infections were performed using mouse-adapted influenza A/Puerto Rico/8/34 (H1N1) virus (IAV), kindly provided by J. A. McCullers (St. Jude Children Research Hospital). Mice were challenged intranasally (in 25 μ l of PBS) with IAV at a sublethal dose of 50 plaque-forming units (p.f.u.) or a median lethal dose (LD $_{50}$) of 100 p.f.u. for the survival experiments. During survival experiments, mice were monitored twice daily for signs of duress and weighed daily. Mice reaching 75% of their original body weight were considered moribund and sacrificed. Viruses were propagated and isolated from Madin–Darby Canine Kidney (MDCK) cells and titrated using standard MDCK plaque assays. MDCK cells were obtained from the American Type Culture Collection (ATCC) and maintained in Dulbecco's modified Eagle's medium (DMEM) enriched with 10% (v:v) fetal bovine serum (FBS), 2 mM L-glutamine and 100 U ml $^{-1}$ of penicillin–streptomycin.

Histopathological analysis

Lungs were inflated with and fixed for 48 h in 10% formalin, then embedded in paraffin. Next, 5-µm sections were cut and stained with hematoxylin and eosin (H&E) or Masson's Trichrome. Slides were scanned at a resolution of ×20 magnification and pictures were taken using a Leica Aperio slide scanner (Leica). Quantification of collagen-afflicted areas on Masson's Trichrome-stained slides was performed using ImageJ software (National Institutes of Health (NIH)).

Flow cytometry

BM or spleen cells (3×10^6 cells) after red blood cell (RBC) lysis were stained with fixable viability dye eFluor-501 (eBioscience) at the concentration of 1:1,000 for 30 min (4 °C). Subsequently, the cells were washed with PBS supplemented with 0.5% BSA (Wisent) and incubated with anti-CD16/32 (clone 93, eBioscience, 1:200) at a concentration of 1:100 in PBS or 0.5% BSA at 4 °C for 10 min except for myeloid progenitor and downstream progenitor staining. The following antibodies were then used for staining: anti-Ter-119 (clone Ter119, 1:100), anti-CD11b (clone M1/70, 1:100), anti-CD5 (clone 53-7.3, 1:100), anti-CD4 (clone RM4-5, 1:100), anti-CD8a (clone 53-6.7, 1:100), anti-CD45R (clone RA3-6B2, 1:100) and anti-Ly6G/C (clone RB6-8C5, 1:100) (all were biotin conjugated and BD Bioscience), added for 30 min at 4 °C. Cells were subsequently washed with PBS or 0.5% BSA. For staining of LKSs, HSCs and MPPs, streptavidin–APC-Cy7 (eBioscience, 1:100), anti-c-Kit-APC (clone 2B8, eBioscience, 1:100), anti-Sca-1-PE-Cy7 (clone D7, eBioscience, 1:100), anti-CD150 eFluor-450 (clone mShad150, eBioscience, 1:100), anti-CD48-PerCP-eFluor-710 (clone HM48-1, BD Bioscience, 1:100), anti-Flt3-PE (clone A2F10.1, BD Bioscience, 1:100)

and anti-CD34-FITC (clone RAM34, eBioscience, 1:100) were added and incubated at 4 °C for 30 min. For staining of myeloid and lymphoid progenitors, streptavidin-APC-Cy7 (eBioscience, 1:100), anti-c-Kit-APC (clone 2B8, eBioscience, 1:100), anti-Sca-1-PE-Cy7 (clone D7. eBioscience, 1:100), anti-CD34-FITC (clone RAM34, eBioscience, 1:100), anti-CD16/32-PerCP-eFluor-710 (clone 93, eBioscience, 1:100) and anti-CD127 BV786 (clone SB/199, BD Bioscience, 1:100) or anti-CD127-BV605 (clone A7R34, BioLegend, 1:100) were added and incubated at 4 °C for 30 min. For cMoPs and downstream progenitors: BM cells were incubated with biotin antibodies against lineage markers as mentioned above, except we included anti-Ly6G (clone 1 A8-Ly6G) to replace anti-Ly6C/6G at 4 °C for 30 min. Cells were subsequently washed with PBS or 0.5% BSA. The following antibodies were added: streptavidin-BUV395 (BD Bioscience, 1:50), anti-c-Kit-Pacific Blue (clone 2B8, BD Bioscience, 1:100), anti-Sca-1-PE-Cy7 (clone D7, eBioscience, 1:100), anti-CD34-FITC (clone RAM34, eBioscience, 1:100), anti-CD16/32-PerCP-efluor-710 (clone 93, eBioscience, 1:100), anti-CD115 BV711 (clone AFS98, BioLegend, 1:100), anti-Flt3-PE (clone A2F10.1, BD Bioscience, 1:100), anti-Ly6C-APC (clone HK1.4, eBioscience, 1:100) and anti-Ly6G AF700 (clone 1 A8-Ly6G, eBioscience, 1:100), and incubated at 4 °C for 30 min. In another set of experiments, cells were fixed and permeabilized using the FOXP3 Transcription Factor Staining Kit (eBioscience) for 1 h at 4 °C. Then, cells were stained with anti-Ki67-PE (clone 16A8, BioLegend, 1:400) for 1 hat 4 °C and acquired.

Staining for innate and adaptive immune cells. RBCs were lysed in BM and collagenase IV (Sigma-Aldrich)-treated lung samples. Lung, spleen or BM cells (3×106) were then stained with fixable viability dye eFluor-501 (eBioscience, 1:1,000) for 30 min (4 °C). Subsequently, the cells were washed with PBS supplemented with 0.5% BSA (Wisent) and incubated with anti-CD16/32 (clone 93, eBioscience. 1:200) in PBS or 0.5% BSA at 4 °C for 10 min. After washing, cells were incubated with fluorochrome-tagged antibodies at 4 °C for 30 min. Antibodies for the innate panel are as follows: anti-CD11b-Pacific Blue (clone M1/70, eBioscience, 1:200), anti-CD11c-PE-Cy7 (clone HL3, BD Bioscience, 1:200), Siglec-F-PE-CF594 (clone E50-2440, BD Bioscience, 1:200), F4/80-APC (clone BM8, eBioscience, 1:200), Ly6C-FITC (clone AL-21, BD Bioscience, 1:200) and Ly6G-PerCP-eFluor-710 (clone 1A8, eBioscience, 1:200). Antibodies for the adaptive panel are as follows: anti-CD3-PE (clone 145-2C11, eBioscience, 1:200), anti-CD19-PE-Cy7 (clone eBio1D3 (1D3), eBioscience, 1:200), anti-CD4-eFluor-450 or anti-CD4-FITC (clone GK1.5, eBioscience, 1:200) and anti-CD8-AF700 (clone 53-6.7, BD Bioscience; 1/200). All cells were subsequently washed with PBS or 0.5% BSA and resuspended in 1% paraformal dehyde.

Blood leukocytes. Whole blood, 50 µl, collected in heparin tubes (BD) was incubated with fluorochrome-tagged antibodies at 4 °C for 30 min. Antibodies for the innate panel are as follows: anti-CD11b-Pacific Blue (clone M1/70, eBioscience, 1:200), anti-CD11c-PE-Cy7 (clone HL3, BD Bioscience, 1:200), anti-Siglec-F-PE-CF594 (clone E50-2440, BD Biosciences, 1:200), anti-F4/80-APC (clone BM8, eBioscience, 1:200), anti-Ly6C-FITC (clone AL-21, BD Bioscience, 1:200) and anti-Ly6G-PerCP-eFluor-710 (clone 1A8, eBioscience, 1:200). Antibodies for the adaptive panel are as follows: anti-CD3-PE (clone 145-2C11, eBioscience, 1:200), anti-CD19-PE-Cy7 (clone eBio1D3 (1D3), eBioscience, 1:200), anti-CD4-FITC (clone GK1.5, eBioscience, 1:200) and anti-CD8 AF700 (clone 53-6.7, BD Bioscience, 1:200). After RBC lysis, cells were subsequently washed with PBS or 0.5% BSA and resuspended in 1% paraformaldehyde. If required, panels were modified to contain anti-CD45.1-APC (clone A20, BD Bioscience, 1:100) and anti-CD45.2-BUV395 (clone 104, BD Bioscience, 1:100). Antibodies were quality checked and validated by the respective manufacturers and information about the validation can be found on the companies' websites. Each antibody has a recommended working concentration found on the associated technical data sheet (for example, BioLegend: suggested

use of this reagent is \leq 0.125 µg per million cells in 100-µl volume). Based on the recommended concentration, the antibody is titrated with cells of interest (lung cells or PBMCs) for optimal performance by flow cytometry. Cells were acquired on the Fortessa-X20 (BD) and analyzed using FlowJo software (v.10.6.1). All percentages are of single viable frequency unless otherwise indicated.

MACSima imaging cyclic staining

Sample preparation and image acquisition. Multiplex immunohistochemistry of lungs from mice 9 d after vehicle or β-glucan injection was performed using a MACSima imaging system (Miltenyi Biotec). Cryosectioned fixed lungs from both groups were mounted on microscopy slides and MACS well sample carriers and blocked using a blocking buffer containing 10% BSA and 2% goat serum for 1 h at 21 °C before nuclei were counterstained with DAPI. The samples were then placed into the MACSima imaging system where they underwent repetitive cycles of immunofluorescent staining, sample washing, multi-field imaging and signal erasure by photobleaching. B cells were identified as B220+ (Miltenyi Biotec, cat. no. RA3-6B2, FITC, 1:50) cells, T cell subsets using antibodies against CD4 (eBioscience, cat no. RM4.5, PE, 1:50) and CD8 (Miltenyi Biotec, cat. no. REA601, PE, 1:50). The neutrophil phenotype was characterized using antibodies to Ly6G (Miltenyi Biotec, cat. no. 1A8, PE,1:50), CD11b (Miltenyi Biotec, cat. no. M1/70, APC, 1:50), CD14 (BioLegend, cat. no. Sa14-2, PE, 1:50), Ly6C (Miltenyi Biotec, cat. no. REA796, PE,1:50), CXCR2 (BioLegend, cat. no. SA044G4, PE, 1:25), CD45 (Miltenyi Biotec, cat. no. REA737, FITC,1:50), MHC-II (Miltenyi Biotec, cat. no. REA813, APC,1:50), CXCR4 (Miltenyi Biotec, cat. no. REA107, PE, 1:50), CD62L (Miltenyi Biotec, cat. no. REA828, APC, 1:50) and CD49d (BD Bioscience, cat. no. MFR4.B, PE, 1:50). The tissue environment was characterized using antibodies to CD31 (polyclonal, R&D, PE, 1:50), LYVE-1 (R&D, cat. no. 223322, PE, 1:50) and SMA (Miltenyi Biotec, cat. no. REAL650, FITC, 1:300).

Data analysis and visualization. For downstream analysis, acquired pictures were first stitched and preprocessed using MACS iQ View Analysis Software (Miltenyi Biotec) before cells were segmented based on the DAPI signal using the StarDist plug-in⁷¹ in ImageJ (NIH) and the donut algorithm in MACS iQ View. The segmented data were then analyzed using MACS iQ View Analysis and FlowJo (BD Biosciences). Neutrophils from all regions of interest were concatenated and phenotypically analyzed by dimensional reduction using the Uniform Manifolld Approximation and Projection (UMAP) plug-in in FlowJo.

Neutrophil spectral flow cytometry phenotyping

Neutrophils were harvested from mice treated with β-glucan (day 0) before influenza infection (day 6), as well as from their respective controls. At the day of sacrifice (day 9), mice were euthanized and blood was harvested and kept on ice. Mice were perfused with ice-cold PBS, their lungs harvested, finely chopped with scissors on ice and filtered to extract leukocytes. Blood and lung samples were then lysed (RBC Lysis Buffer, BioLegend, cat. no. 420301) and kept on ice. Samples were then stained on ice with CD45-PerCP (clone 30-F11, BioLegend), Ly6G-BUV395 (clone 1A8, BD Bioscience), CD101-APC (clone Moushi101, eBioscience), CXCR2-PE (clone SA044G4, BioLegend), CXCR4-BV711 (clone L276F12, BioLegend), CD62L-BV480 (clone MEL-14, BD Bioscience), CD24-AF700 (clone M1/69, BioLegend), CD117-BV421 (clone 2B8, BioLegend), CD11b-BUV496 (clone M1/70, BD Bioscience), CD49d-BUV563 (clone 9C10, BD Bioscience), CD44-BV570 (clone IM7, BioLegend), CCR2-BV750 (clone 475301, BD Bioscience), Ly6C-BV785 (clone HK1.4 BioLegend), CD80-BV650 (clone M18/2, BD Bioscience), MHC-II-BUV661 (clone M5/114, BD Bioscience), CD16-PE/Dazzle594 (clone S17014E, BioLegend), CD115-AF488 (clone AFS98, BioLegend) and CD14 APC/Fire780 (clone Sa14-2, BioLegend) in staining buffer (BioLegend, cat. no. 420201). Samples were acquired using an Aurora spectral flow cytometer (five-laser configuration, Cytek). Data were analyzed using FlowJo. In brief, Cd11b $^+$ Ly6G $^+$ neutrophils from all mice were concatenated to perform UMAP, followed by Flowsom clustering using 17 surface markers (CD45, Ly6G, CD101, CXCR2, CXCR4, CD62L, CD117, CD24, CD11b, CD49d, CD44, CCR2, Ly6C, CD80, MHC-II, CD16 and CD14).

Protein and erythrocytes in BAL

BAL was collected by cannulating the trachea with a 22-gauge cannula, then washing the lungs with $3\times1\,\text{ml}$ of cold sterile PBS. The total volume recovered after lavage was -0.7 ml. Samples were spun down (1,500 rpm for 10 min). Cells were used to assess the number of erythrocytes and the total protein content in the supernatant was assessed by Pierce BCA Protein assay (Thermo Fisher Scientific).

Endothelial permeability

Infected or uninfected mice were injected i.p. with 400 μ l of Evans Blue dye (2% in PBS). After 1 h, mice were euthanized, the BAL collected and the lungs perfused with 10 ml of PBS. Evans Blue was then extracted by overnight incubation in 50% trichloroacetic acid at 4 °C (BAL) and quantified by spectrophotometric analysis using a standard curve of Evans Blue in 50% trichloroacetic acid.

Wet:dry ratio

Lungs were harvested from naive or IAV-infected mice (50 p.f.u.; day 6 post-infection) and blood clots were carefully removed. Then, the lungs were weighed (wet weight) and dried in an oven (56 $^{\circ}$ C, 2 d, dry weight), and the dry weight measured. Data are presented as the ratio wet weight:dry weight.

Evaluation of mitochondrial mass using Mitotracker Green

Single-cell suspensions were stained with extracellular antibodies as described above and then with Mitotracker Green 150 nM (Invitrogen technologies) in PBS for 30 min at 22 $^{\circ}$ C, then washed with PBS.

Intravascular staining

Mice were given 2 µg of FITC-conjugated anti-CD45.2 i.v. After 2 min, mice were euthanized and the lungs were collected and stained ex vivo with BUV737-conjugated anti-CD45.2 antibody to determine the parenchymal or vascular localization of the cells.

Purification of neutrophils

Neutrophils were purified from the blood, spleen or BM using the EasySep Mouse Neutrophils Enrichment Kit following the manufacturer's instructions (Stem Cell Technology).

Adoptive transfer model

Neutrophils were purified from BM of control or β -glucan-treated CD45.1 mice using the EasySep Mouse Neutrophil Cell Isolation Kit (Stem Cell Technologies) according to the supplier's recommendations. Isolated cells were counted and washed (in cold sterile PBS). Purity was verified by flow cytometry and was always >75% neutrophils before transfer. A total of 3×10^6 neutrophils in 100 μ l of PBS was transferred into naive CD45.2 mice via the intravenous route. Mice were infected the following day with a lethal dose of IAV (120 p.f.u.) and monitored for survival.

Extracellular flux analysis

Real-time OCRs of purified neutrophils from blood were measured in XF medium (non-buffered DMEM containing 2 mM L-glutamine, 25 mM glucose and 1 mM sodium pyruvate) using a Seahorse Xfe 96 Analyzer (Agilent Technologies). For the mitochondrial stress test, mitochondrial inhibitors oligomycin, FCCP, antimycin A and rotenone were used as per the manufacturers' recommendations. Neutrophils were purified as described above. Neutrophil adherence was achieved by plating a suspension of sorted neutrophils in Seahorse assay medium

with 2 mM glutamine and 25 mM glucose, and spinning at the lowest acceleration to 45g followed by natural deceleration. Sorted neutrophils were seeded at 0.2×10^6 cells per well and incubated for 1 h at $37\,^{\circ}\text{C}$ with no CO $_2$. XF analysis was performed at $37\,^{\circ}\text{C}$ with no CO $_2$ using the XF-96e analyzer (Seahorse Bioscience) as per the manufacturer's instructions. All measurements were normalized to the cell number using a Crystal Violet dye extraction assay. OCRs were generated using Wave Desktop 2.3 (Agilent Technologies). Basal OCR was calculated by subtracting measurement 7 (nonmitochondrial respiration) from measurement 1. Maximal respiration was calculated by subtracting measurement 7 (nonmitochondrial respiration) from measurement 5 and spare respiratory capacity was the difference between maximal respiration and basal rate.

Intravital microscopy

Lung intravital microscopy was performed as previously described⁷². Fluorescently conjugated anti-CD45 monoclonal antibody (5 µg, clone 30-F11) was administered i.v. to discriminate intravascular leukocytes from nonintravascular leukocytes. Neutrophils were quantified using Imaris as either intravascular (TdTom⁺CD45⁺) or parenchymal (TdTom⁺CD45⁻). To visualize mitochondrial high neutrophils, Mitotracker Green was administered i.v. just before imaging.

Bulk RNA-seq

Experimental mice were split into two groups (either infected with IAV or β -glucan treated + IAV) with four animals each. Then, 7 d after treatment, animals were infected with IAV and, on day 6 post-infection, neutrophils were purified from the spleen using the EasySep Neutrophil Enrichment Kit and RNA was extracted using an RNeasy kit (QIAGEN) according to the manufacturer's instructions.

RNA-seq data processing. Adapter sequences and low-quality score bases were first trimmed using Trimmomatic with parameters -phred33 SE ILLUMINACLIP:TruSeq3-SE.fa:2:30:10 LEADING:3 TRAILING:3 SLID-INGWINDOW:4:15 MINLEN:36 (ref. 73). The resulting reads were aligned to the mm10 mouse reference genome using STAR⁷⁴. Read counts are obtained using featureCounts⁷⁵ with default parameters.

Differential gene expression analyses. Gene expression levels across all samples were first normalized using the calcNormFactors function implemented in the edgeR package (v.3.34.0), which utilizes the TMM algorithm (weighted trimmed mean of M values) to compute normalization factors. Then, the voom function implemented in the limma package (v.3.38.3) was used to log(transform) the data and calculate precision weights. A weighted fit using the voom-calculated weights was performed with the ImFit function from limma. The effects of β-glucan on baseline gene expression and of β-glucan priming on response to subsequent influenza infection were: normalized, log(transformed) gene expression levels for each sample were fit to the linear model Expression ~1 + primary + secondary:primary, where primary refers to the absence or presence of β-glucan priming and secondary to the uninfected or IAV-infected conditions. This model captures the independent effect of β-glucan exposure on gene expression as well as the response of primed and nonprimed samples to IAV infection. The make Contrasts and contrasts.fit functions implemented in limma were used to compare the gene expression response to influenza in naive neutrophils with that of β-glucanexposed neutrophils.

GSEA. GSEAs were performed using the fgsea R package (v.1.18.0) with parameters: minSize = 15, maxSize = 500, nperm = 100,000. To investigate pathway enrichments among genes with altered responses to IAV infection before compared with after β -glucan priming, genes were ordered by the rank statistic: $-\log 10(P) \times \log(fold\text{-change})$ and compared with the Reactome gene sets from the MSigDB collections.

GO pathway enrichments and visualization. Gene ontology (GO) enrichment analyses for genes with a response to IAV infection modulated by β -glucan priming (P < 0.05) were performed and visualized using the ClueGO application of Cytoscape⁷⁶.

ScRNA-seq

Data generation. Lungs were harvested from control and β-glucantreated mice and mechanically disrupted with scissors before being treated with collagenase type I, DNase I and elastase (Worthington) for 30 min at 37 °C. Cells were then passed through a 100-μm cell strainer and RBCs were lysed. Single-cell suspensions were stained with TotalSeq-tagged anti-CD45 and anti-Ly6G (BioLegend) according to the manufacturer's instructions. Single-cell GEX (gene expression) and CSP libraries were generated using a Chromium Controller instrument (10x Genomics). Sequencing libraries were prepared using Chromium Single Cell 3'-Reagent Kits (10x Genomics), according to the manufacturer's instructions. GEX libraries were amplified with a thermal cycler for 13 cycles and CSP libraries for 10 cycles.

ScRNA-seq preprocessing and analysis. FASTQ files from each library were mapped to the GRCm39 reference genome using Cell-Ranger (v.7.0). Then Seurat (v.4.3.0.1, R v.4.3.1) was used to perform quality control filtering of cells. In total, we captured 44,045 cells before filtering. Cells were retained for downstream analysis if they had: (1) between 200 and 3,000 UMIs detected (nFeature_RNA), (2) <10,000 total molecules detected per cell (nCount RNA) and (3) a mitochondrial read percentage <5%, leaving 29,983 cells. After quality control, libraries were merged using merge(), then normalized and scaled using Seurat's SCTransform function. Then, dimensionality reduction was performed via principal component analysis (PCA) (RunPCA function) and UMAP (RunUMAP function, dims = 1:15). A shared nearest neighbor (SNN) graph was built using the FindNeighbors function (dims = 1:20) and, finally, clusters were called with the FindClusters function (resolution = 0.1). The neutrophil cluster was identified based on positive expression of both Ly6g transcript and LY6G protein. This cluster was further confirmed by using the AddModuleScore function to generate a 'neutrophil score' composed of neutrophil-specific genes⁷⁷. We then reclustered the neutrophils and, before analysis, small clusters, probably containing doublets, with cell counts <10 cells per condition, high feature numbers and high levels of transcripts indicative of B and T cells were removed from downstream analysis. After this additional quality control, 925 cells remained. These cells were renormalized and rescaled, followed by dimensionality reduction, SNN graph generation and clustered as above. UMAP visualization was performed using dittoSeq2 (v.1.14.3), followed by differential expression analysis (non-treated control versus day 4 and non-treated control versus day 7) using FindMarkers() to identity DEGs (adjusted P < 0.05) in response to β -glucan stimulation⁷⁸.

Statistical analysis

Data are presented as mean \pm s.e.m. Statistical analyses were performed using GraphPad Prism v.1.0 software. Statistical differences were determined using two-sided log(rank) test (survival studies), one-way ANOVA followed by Šidák's multiple-comparison test, two-way analysis of variance (ANOVA) followed by Šidák's or Dunnett's multiple-comparison test, two-tailed, unpaired Student's t-test or two-tailed Mann–Whitney U-test. Data distribution was assumed to be normal but this was not formally tested. Data collection and analysis were not performed blind to the conditions of the experiments.

Ethics statement

All experiments involving animals were approved by McGill (permit no. 2010-5860) in strict accordance with the guidelines set out by the Canadian Council on Animal Care.

Reporting summary

Further information on research design is available in the Nature Portfolio Reporting Summary linked to this article.

Data availability

ScRNA-seq data have been deposited on the Gene Expression Omnibus under accession no. GSE269104. Source data are provided with this paper.

References

- Schmidt, U., Weigert, M., Broaddus, C. & Myers, G. Cell Detection with Star-Convex Polygons. In International Conference on Medical Image Computing and Computer-Assisted Intervention 265–273 (Springer International Publishing, 2018).
- 72. Yipp, B. G. et al. The lung is a host defense niche for immediate neutrophil-mediated vascular protection. Sci. Immunol. 2, eaam8929 (2017).
- Bolger, A. M., Lohse, M. & Usadel, B. Trimmomatic: a flexible trimmer for Illumina sequence data. *Bioinformatics* 30, 2114–2120 (2014).
- 74. Dobin, A. et al. STAR: ultrafast universal RNA-seq aligner. *Bioinformatics* **29**, 15–21 (2013).
- Liao, Y., Smyth, G. K. & Shi, W. featureCounts: an efficient general purpose program for assigning sequence reads to genomic features. *Bioinformatics* 30, 923–930 (2014).
- Shannon, P. et al. Cytoscape: a software environment for integrated models of biomolecular interaction networks. *Genome Res.* 13, 2498–2504 (2003).
- Xie, X. et al. Single-cell transcriptome profiling reveals neutrophil heterogeneity in homeostasis and infection. *Nat. Immunol.* 21, 1119–1133 (2020).
- Bunis, D. G., Andrews, J., Fragiadakis, G. K., Burt, T. D. & Sirota, M. dittoSeq: universal user-friendly single-cell and bulk RNA sequencing visualization toolkit. *Bioinformatics* 36, 5535–5536 (2021).

Acknowledgements

We acknowledge technical help from staff at the Research Institute of the McGill University Health Centre (RI-MUHC) histopathology platform, and thank M. Orlova for the scRNA-seq. This work was supported by a Canadian Institute of Health Research (CIHR) project grant (no. 168885), grant no. NIH-UO1-AI160406, and Bill and Melinda

Gates Foundation (grant no. INV-003360) to M.D. M.D. holds a Fonds de Recherche du Québec—Sante Award and the Strauss Chair in Respiratory Diseases and is a fellow member of The Royal Society of Canada. N.K. was supported by a Fonds de Recherche du Québec—Sante Fellowship and a CIHR fellowship. K.A.T. is supported by a Fonds de Recherche du Québec—Sante doctoral studentship. O.S. receives funds from the German Research Foundation (DFG; grant no. CRC TRR332, project nos. A2 and Z1 and project 502158695). R.C. receives support from the Innovative Medical Research of the Medical Faculty of the University of Münster. The funders had no role in study design, data collection and analysis, the decision to publish or the preparation of the manuscript.

Author contributions

M.D. and N.K. conceived the project and designed the experiments. N.K., K.A.T., R.C., M.R., A.H., S.S., M.S., E.P., E.K., A.G., A.S., J.D., O.S. and B.G.Y. performed the experiments. N.K., K.A.T., R.C., S.S., S.A.K. and V.L. analyzed and discussed the data. L.B. V.L. and S.S. performed RNA-seq bioinformatics analysis. P.J. performed the histopathology scoring. N.K., K.A.T. and M.D. wrote the paper. M.D. supervised the project.

Competing interests

The authors declare no competing interests.

Additional information

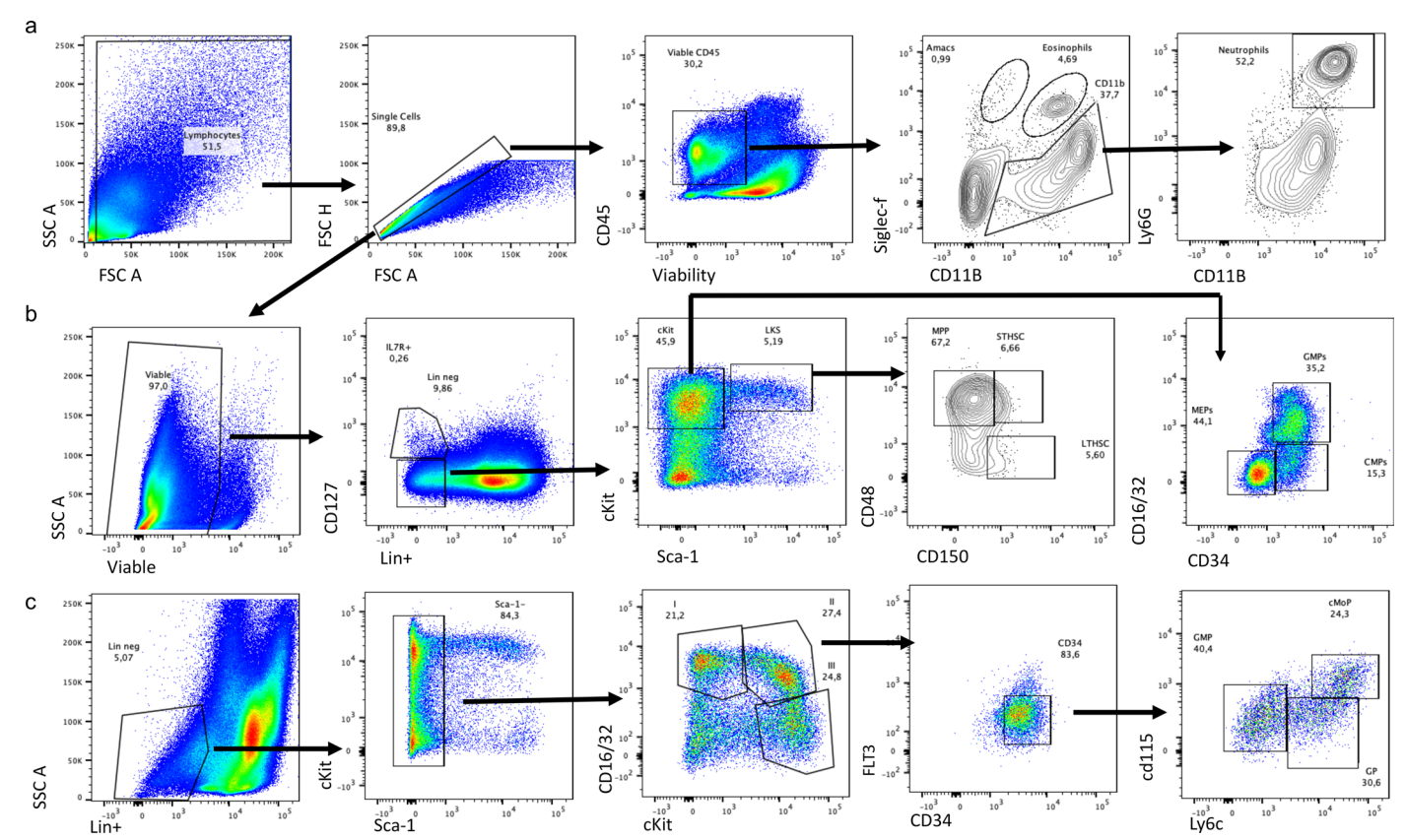
Extended data is available for this paper at https://doi.org/10.1038/s41590-024-02041-2.

Supplementary information The online version contains supplementary material available at https://doi.org/10.1038/s41590-024-02041-2.

Correspondence and requests for materials should be addressed to Nargis Khan or Maziar Divangahi.

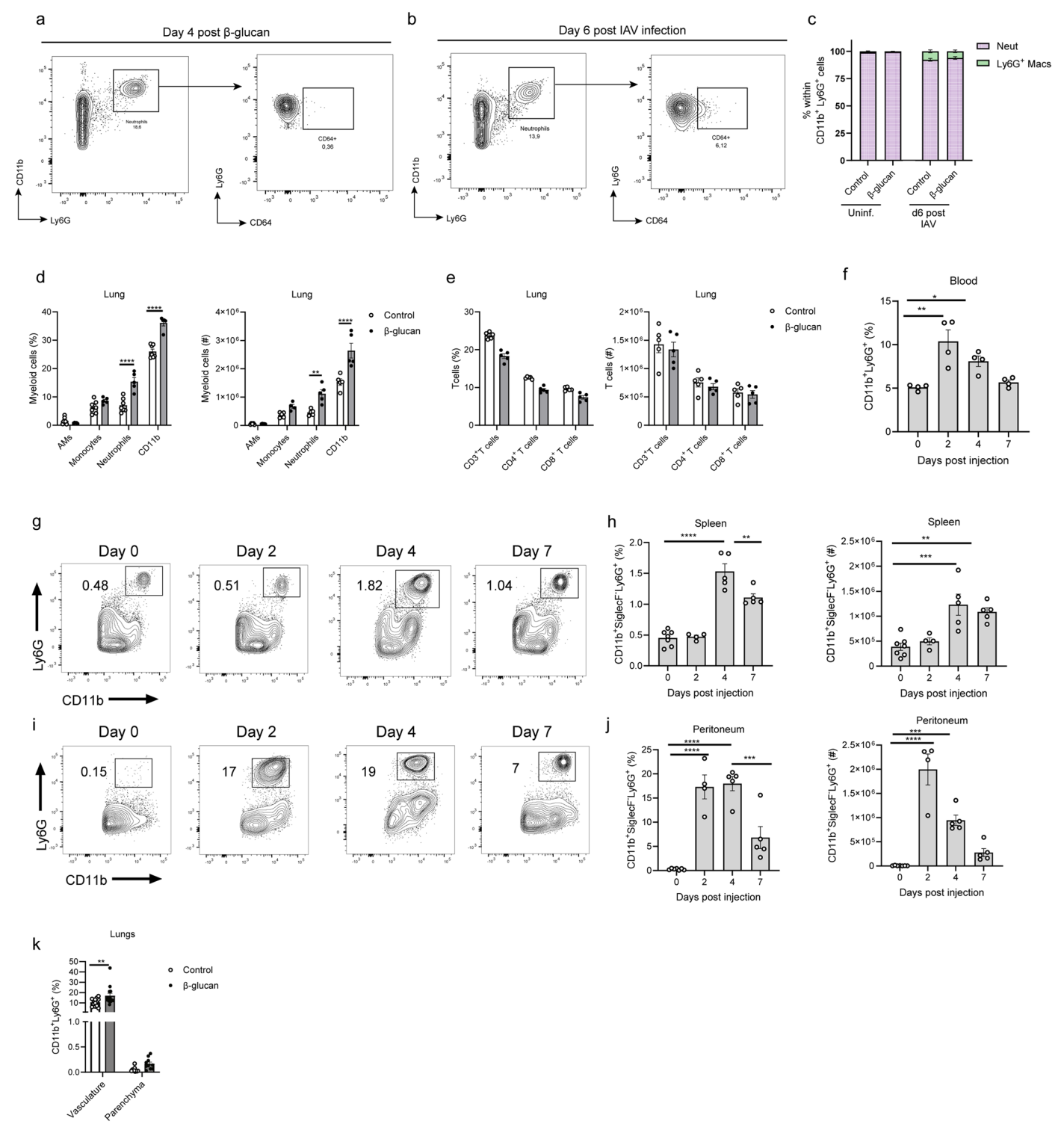
Peer review information *Nature Immunology* thanks Ivan Ballesteros, Andrew Luster and the other, anonymous, reviewer(s) for their contribution to the peer review of this work. Primary Handling Editor: L. A. Dempsey, in collaboration with the *Nature Immunology* team.

Reprints and permissions information is available at www.nature.com/reprints.



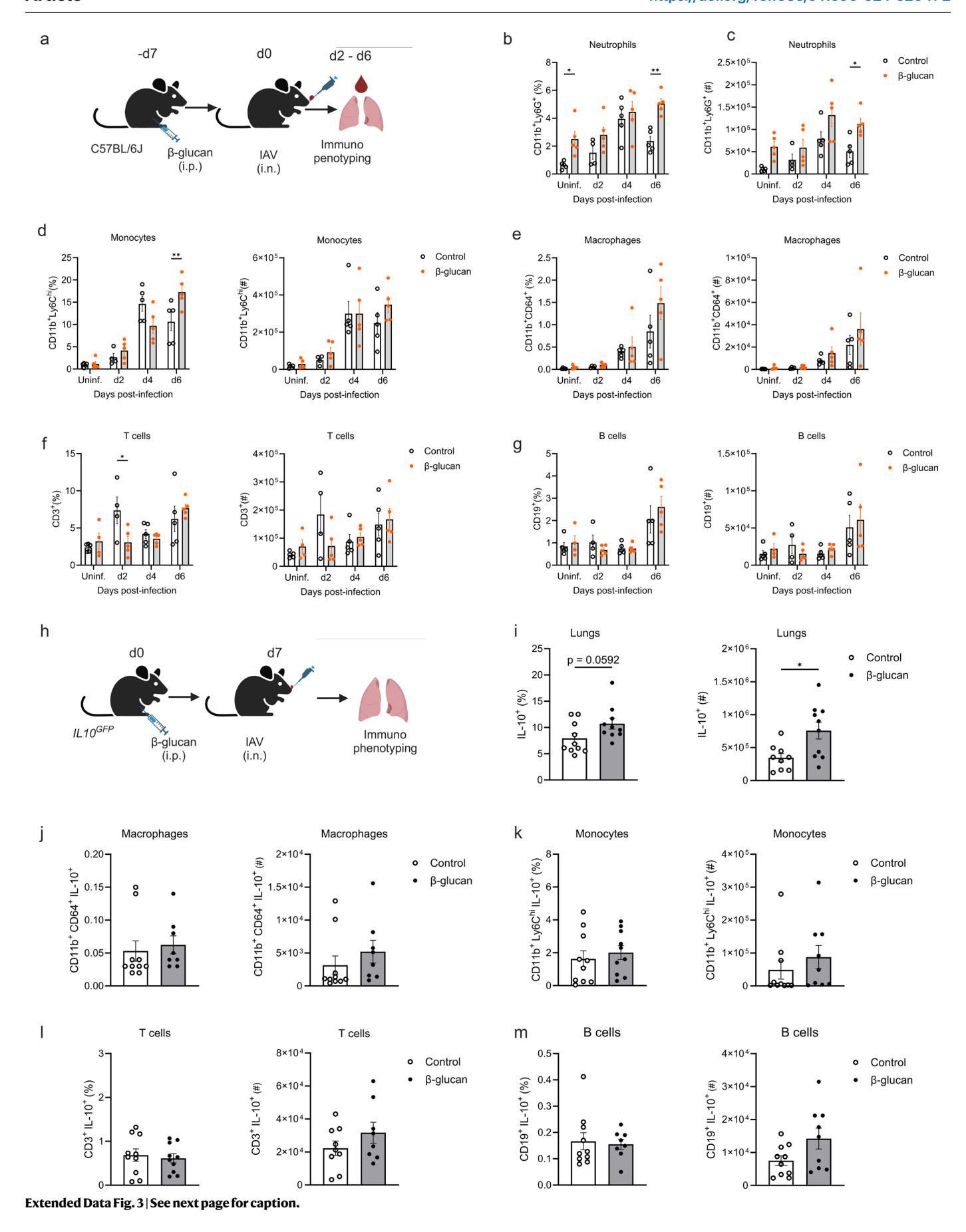
Extended Data Fig. 1| **Gating Strategy. (a)** Cells were gated for FSC-A against SSC-A. Doublets were excluded using FSC-H against FSC-A. Viable CD45+ cells were gated, and within the viable CD45+ cells, cells were gated as CD11b, excluding SiglecF+ cells. CD11b and Ly6G double-positive cells were gated as neutrophils. **(b)** Cells were gated for FSC-A against SSC-A and doublets were excluded using FSCH against FSC-A as shown in **(a)**. Viable cells were gated, and lineage-committed cells were excluded. Within the lineage-negative population, cells were gated as CD127+ and CD127-. Lin-CD127- population was further gated as LKS-defined as double positive for cKit and Sca-1, and cKit is gated as Sca-1

negative and cKit positive. Gated on the LKS population, cells were divided into LT-HSC, STHSC and MPP based on CD150 and CD48 expression. C-Kit+ Sca-1- cells were further gated based on CD34 and CD16/32 to define CMP, GMP and MEP. (c) Finally, in another set of experiments, Lineage+ cells and then Sca-1+ cells were excluded. The remaining cells were subdivided into cKit+ CD16/32+ (II) and cKit+ CD16/32- groups. In the cKit+CD16/32+, cells were further gated on CD34+ Flt3- cells. Within this fraction, Ly6C + CD115- cells were the GP, and Ly6C + CD115+ were cMoP.



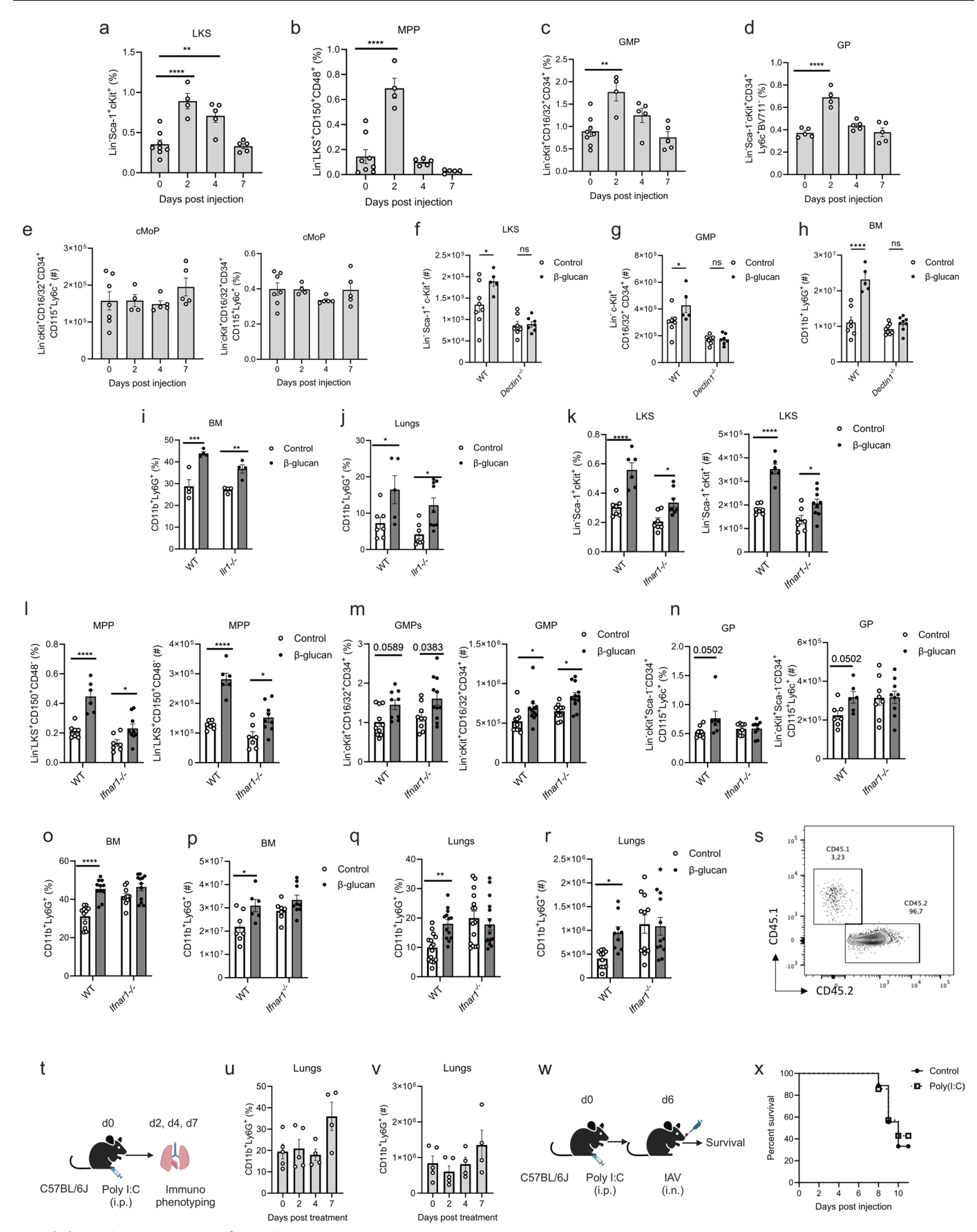
Extended Data Fig. 2 | β-glucan treatment promotes granulopoiesis. (a) Representative FACS plots for CD64 expression on gated CD11b $^+$ Ly6G $^+$ neutrophils at 4 days post β-glucan, and (b) 6 days post-IAV infection. (c) Frequency of Ly6G $^+$ CD64 $^+$ macrophages within CD11b $^+$ Ly6G $^+$ cells (n = 5). Mice were treated with β-glucan and immune cells were assessed on day 4 in the lungs. Frequency and total cell count of myeloid cells (d); and adaptive cells (e) in the lungs of β-glucan-treated mice. (f-j) Kinetics of neutrophils in the blood

(f) spleen (\mathbf{g}, \mathbf{h}) and peritoneum (\mathbf{i}, \mathbf{j}) post β -glucan treatment. FACS plots show indicates the frequency of viable cells. (\mathbf{k}) Intravascular staining at day 4 post- β -glucan treatment. Frequency of neutrophils in the vasculature and parenchyma of the lungs (n=5). Data represented as mean \pm SEM. Data were analyzed using one-way ANOVA followed by Sidak's multiple comparisons tests $(\mathbf{f}, \mathbf{h}, \mathbf{j})$ or two-way ANOVA followed by Sidak's multiple comparisons tests $(\mathbf{d}, \mathbf{e}, \mathbf{k})$. * p < 0.005, *** p < 0.001, **** p < 0.0001.



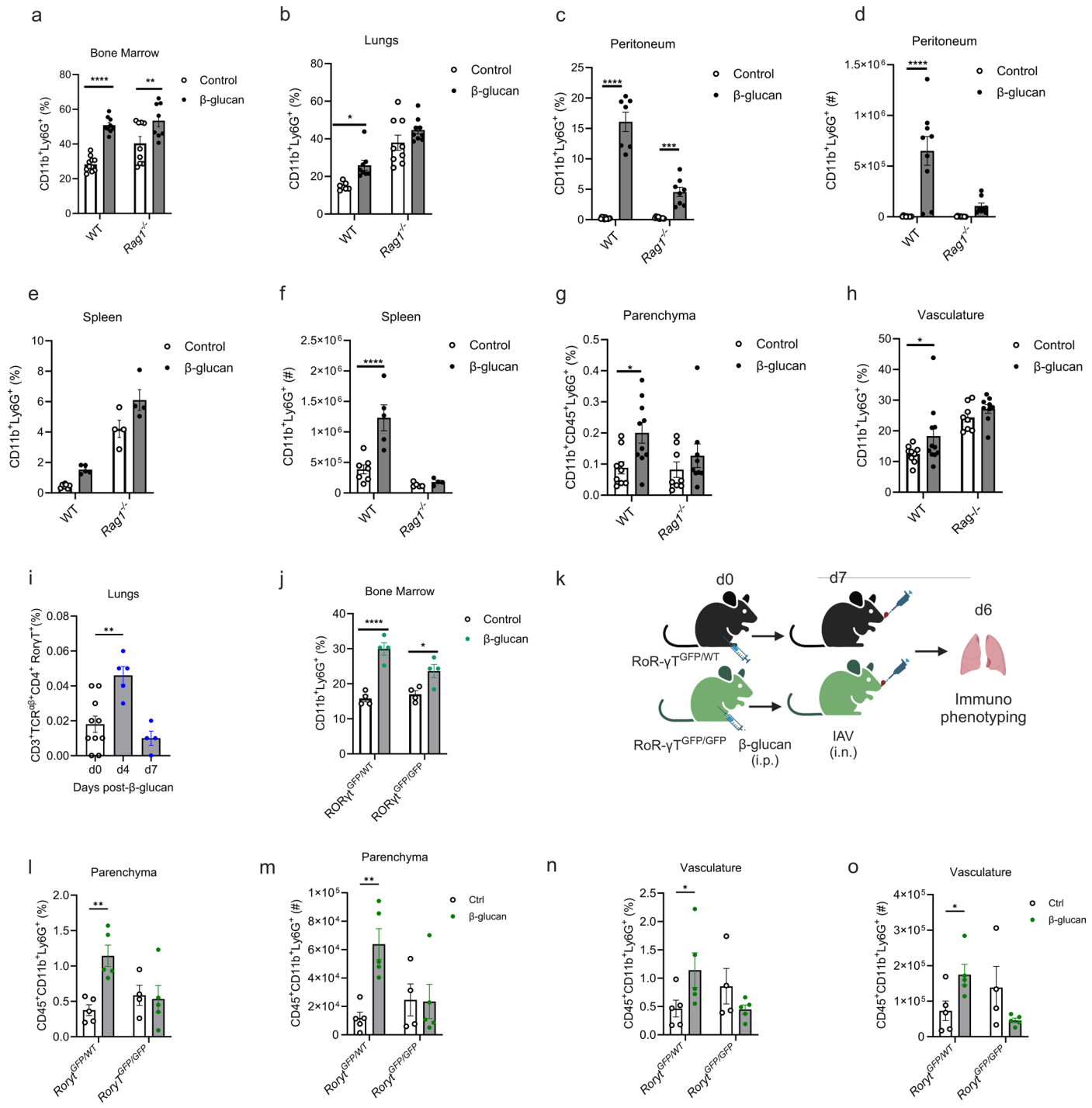
Extended Data Fig. 3 | β -glucan treatment does not induce the expansion of other immune cells following IAV infection. (a) Mice were infected with IAV at day7 post β -glucan treatment. Frequency and total cell number in the lung parenchyma of neutrophils (**b**, **c**), monocytes (**d**), macrophages (**e**), T cells (**f**) and B cells (**g**) (n = 5). (**h**) $ll10^{GFP}$ reporter mice were infected with IAV at day7 post β -glucan treatment. Lungs were collected 6 days post IAV-infection. Frequency

and total cell number of $\emph{Il10}$ -expressing cells (i), macrophages (j), monocytes (k), T cells (l) and B cells (m) in the lungs (n = 9). Data represented as mean \pm SEM. Data were analyzed using two-tailed unpaired t-test (i-m) or two-way ANOVA followed by Sidak's multiple comparisons tests(b-g).* p < 0.05, **p < 0.01, **** p < 0.001, **** p < 0.001. Illustrations in a and h created using BioRender.com.



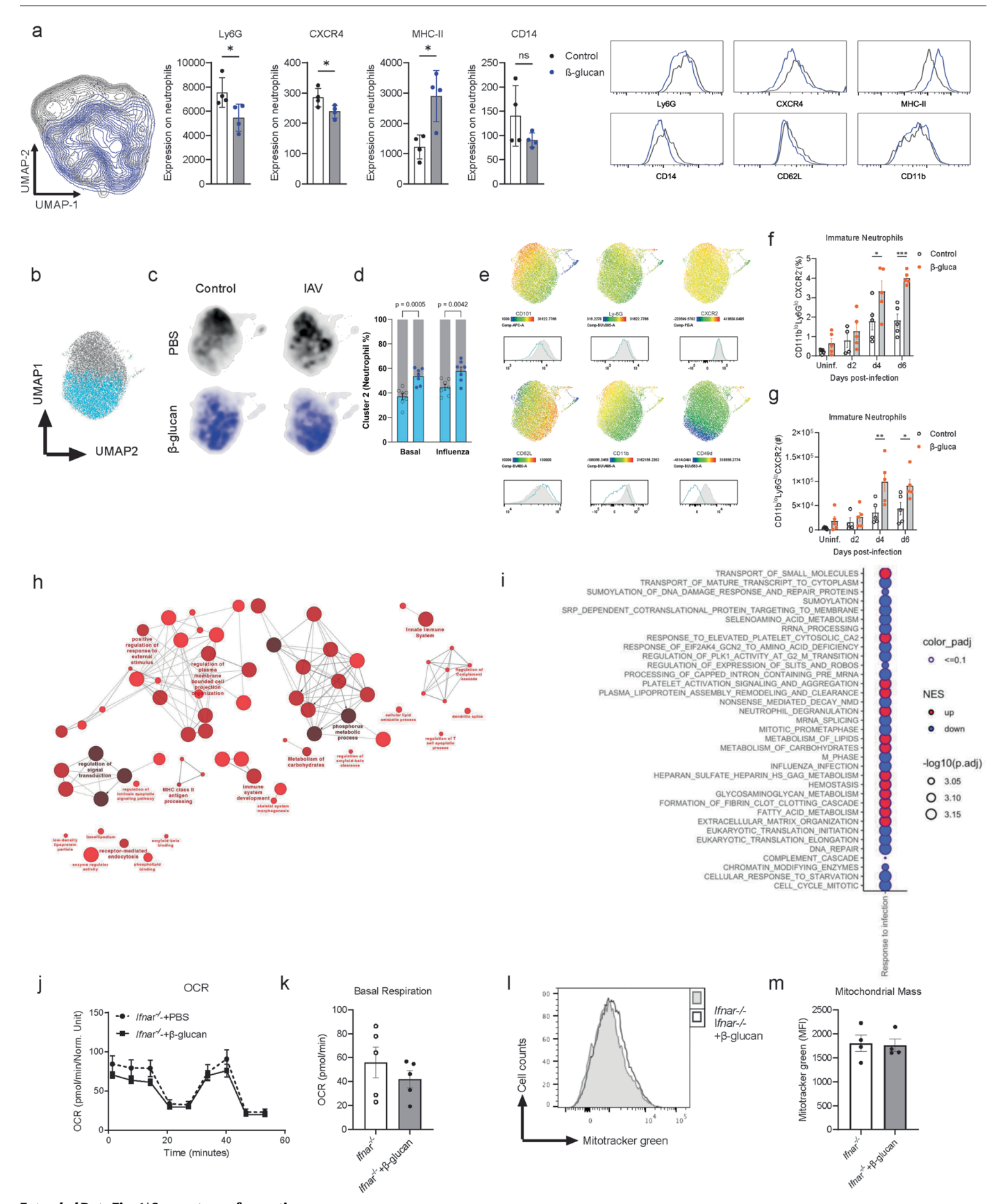
Extended Data Fig. 4 | See next page for caption.

Extended Data Fig. 4 | β-glucan-driven granulopoies is is dependent on type IIFN signalling. (a-e) Kinetics of LKS/progenitors in the BM of β-glucan treated mice. Frequency of LKS (a), MPP (b), GMP (c), GP (d), cMoP (e) in the BM of β-glucan treated mice (n = 4, data pooled from two individual experiments). (f-h) Dectin-1^{-/-} mice were treated with β-glucan. Total cell number of LKS (f), GMP (g) and neutrophils (h) at day 4 (n = 5). C57BL/6 (WT and $IIIr^{-/-}$) mice were treated with β-glucan. Frequency of neutrophils in the BM (i); and lungs (j) of β-glucan treated mice at day 4. (k-r) WT and IIInarIr-/- mice were treated with β-glucan. Frequency and total cell counts of LKS (k); MPP (l); GMP (m); and GP (n) in the BM at day 4 post-glucan treatment (n = 5). Frequency of neutrophils



Extended Data Fig. 5 | Localization of trained neutrophils is dependent on adaptive immune cells. (a-h) C57BL/6 (WT and $Rag1^{\prime}$) mice were treated with β -glucan. Frequency of neutrophils in the BM (a) and lungs (b); frequency and total cell counts of neutrophils in the peritoneum (c, d); spleen (e, f) at day 4 post-glucan treatment. Frequency of neutrophils in the parenchyma (g) and vasculature (h) of lungs at day 4 post β -glucan treatment (n = 4, data pooled from two individual experiments). (i) Mice were treated with β -glucan, frequency of Roryt cells CD4* were quantified at several timepoints post-treatment (n = 5). (j) RORyt GFP/GFP or RORyt WT/GFP mice were treated with β -glucan. Frequency of

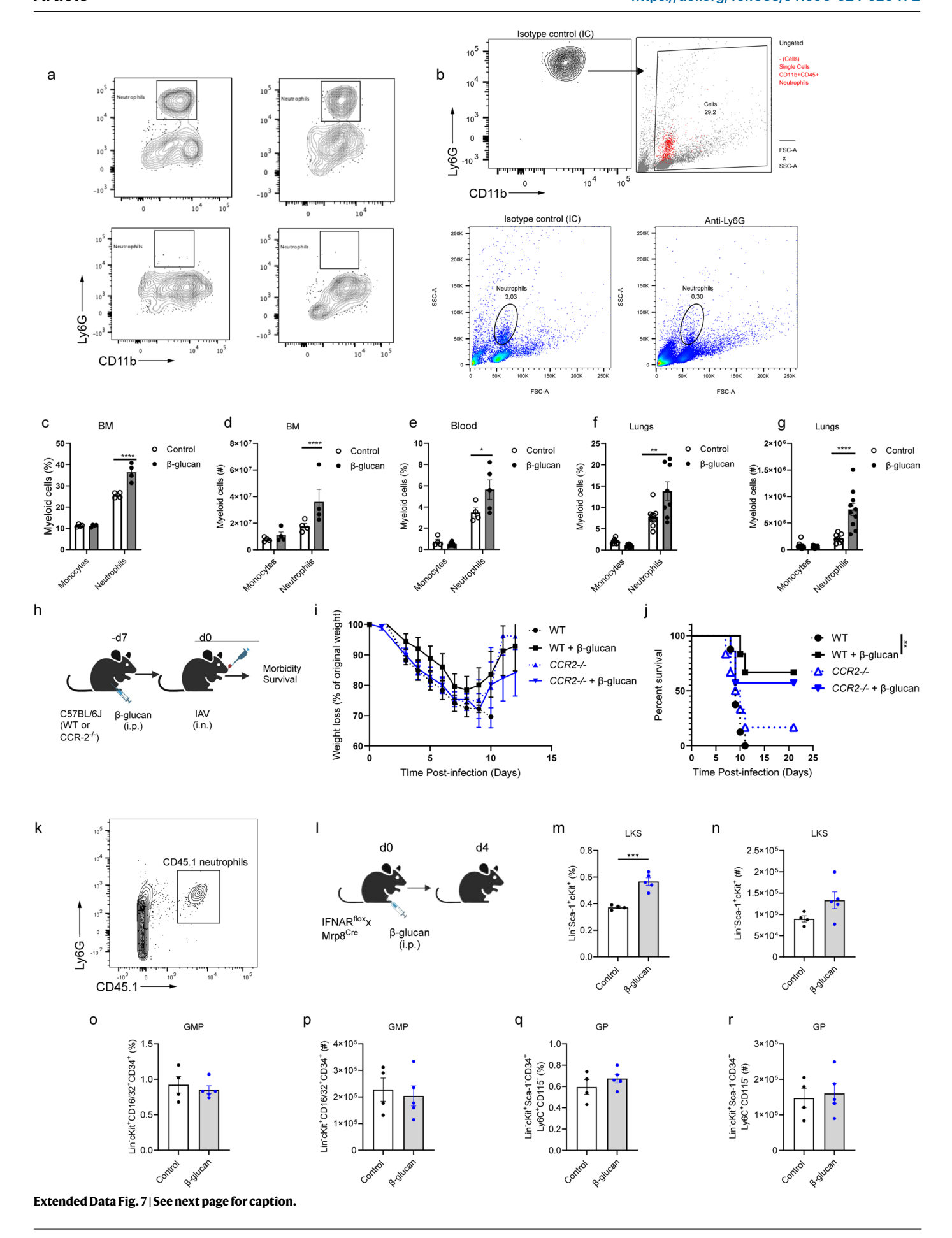
neutrophils in the BM at day 4 post-glucan treatment (n = 4). (k) ROR $\gamma t^{GFP/GFP}$ or ROR $\gamma t^{WT/GFP}$ mice were infected with IAV at day 7 post β -glucan. Frequency and total cell counts of neutrophils were quantified in the lung parenchyma (1, m) and vasculature (n, o) at day 6 post-IAV infection (n = 4). Data represented as mean \pm SEM. Data were analyzed using one-way ANOVA followed by Sidak's multiple comparisons tests (i) or two-way ANOVA followed by Sidak's multiple comparisons tests (a-h,j,l-o). *p < 0.05, **p < 0.01, **** p < 0.001, **** p < 0.0001. Illustration in k created using BioRender.com.



Extended Data Fig. $6\,|\,See$ next page for caption.

Extended Data Fig. 6 | β-glucan treatment augments mitochondrial respiration. (a) UMAP of CD11b⁺Ly6G⁺ neutrophils from control and β-glucantreated mice with relative expression of surface markers quantified by MACSima segmentation 4 days post β -glucan (n = 4). (**b-e**) Mice were treated with β -glucan and infected with IAV after 6 days. 9 days post β-glucan treatment, blood neutrophils were purified and analyzed for spectral flow cytometry. (b) UMAP of CD11b⁺Ly6G⁺ neutrophils from the blood of control and β-glucan treated mice with and without influenza infection. Neutrophils separate in two main Flowsom Clusters (cluster 1, grey and cluster 2, Cyan, 96% of neutrophils) (c) UMAP from A is projected for the 4 experimental group (PBS+/- Influenza, black and β-glucan +/- Influenza, Dark Blue). Neutrophil density repartition shows a shift of neutrophils in β -glucan treated group from Cluster 1 to Cluster 2. (d) Quantification of neutrophil repartition. (e) MFIs of selected markers are projected on the UMAP from (b). Histograms show MFIs from Cluster 1 (grey) and cluster 2 (Cyan). Cluster 2 neutrophils exhibit lower expression of classical maturation markers CD101, Ly6G and CXCR2 and present with a less activated phenotype (CD62Lhigh, CD11blow, CD49dlow) (n = 7). (f, g) Mice were infected with IAV at day 7 post β-glucan. Frequency and counts of immature neutrophils were quantified at several days post-IAV infection (n = 5). (h, i) Mice were infected with IAV at day 7 post β-glucan. Splenic neutrophils were purified at

day 4 post IAV and subjected to Bulk-RNAseq. (h) Network visualization of GOterms significantly enriched among genes whose response to IAV was primed by β -glucan exposure (p < 0.05). Each circle represents an enriched GO term (p.adj < 0.05). The larger nodes with darker shading indicate a greater degree of significance. Connections between nodes indicate similarity between terms. (i) Summary bubble plot of gene set enrichment analysis (GSEA) results. Genes were ordered by the rank statistic –log10(pval)*logFC for the effect of β -glucan priming on response to IAV infection and compared against Reactome gene sets. Circle size and shading is scaled to the normalized enrichment score (NES). All circles with a dark border have $p_{adi} < =0.1$. Red circles indicate that the pathway is increased in β -glucan primed samples and blue circles indicate that β -glucanpriming leads to an overall decrease in expression of the pathway. (**i-m**) *Ifnar1*^{-/-} mice were treated with β-glucan. Neutrophils were purified from blood on day 4 post β-glucan treatment. Neutrophils' cellular metabolism was determined by seahorse (j) and basal respiration (k). Representative histogram plot (l) and quantification (MFI) for mitochondrial mass (**m**) using mitotracker green dye in the neutrophils from the lungs of β -glucan-treated *Ifnar1*^{-/-} mice (n = 4). Data represented as mean \pm SEM. Data were analyzed using two-tailed unpaired t-test (a,k m) or two-way ANOVA followed by Sidak's multiple comparisons tests (j, f, g). *p < 0.05, **p < 0.01, ***p < 0.001, ****p < 0.0001.



Extended Data Fig. 7 | β-glucan mediated protection depends on trained neutrophils. (a) FACS plots showing the depletion of neutrophils in the blood of mice treated with anti-LY6G depletion antibody based on Ly6G and CD11b expression. (b) FACS plots showing the depletion of neutrophils based on FSC/SSC back gating. (c-g) WT and $Ccr22^{f}$ mice were treated with β-glucan. Frequency and absolute number of monocytes and neutrophils in the BM (c, d); blood (e); and lungs (f, g) at day 4 post β-glucan treatment (n = 4, data pooled from two individual experiments). (h-j) C57BL/6 (WT and $Ccr2^{f}$) mice were infected with IAV (lethal dose) at day 7 post β-glucan treatment. Weight loss (i) and survival (j)

was monitored over time (n = 10). (**k**) Adoptive transfer of CD45.1 neutrophils confirmed in the lungs of CD45.2 recipient mice. (**I-m**) IFNAR^{flox} x Mrp8^{Cre} mice were treated with β -glucan for 4 days, frequency and total cell counts of LKS⁺ cells (**m**, **n**), GMPs (**o**, **p**) and GPs (**q**, **r**) were quantified in the BM (n = 4). Data represented as mean \pm SEM. Data were analyzed using two-tailed unpaired t-test (**m-r**) or two-way ANOVA followed by Sidak's multiple comparisons tests (**c-g**, **i**). Survival was monitored by a log-rank test (**j**). * p < 0.05, ** p < 0.01, **** p < 0.001. Illustrations in **h** and **l** created using BioRender.com.

nature portfolio

Corresponding author(s):	Maziar Divangahi and Nargis Khan
Last updated by author(s):	Nov 19, 2024

Reporting Summary

Nature Portfolio wishes to improve the reproducibility of the work that we publish. This form provides structure for consistency and transparency in reporting. For further information on Nature Portfolio policies, see our Editorial Policies and the Editorial Policy Checklist.

For all statistical analyses, confirm that the following items are present in the figure legend, table legend, main text, or Methods section.

_				
5	ta	ŤΙ	ıst	ics

n/a	Confirmed
	$oxed{\boxtimes}$ The exact sample size (n) for each experimental group/condition, given as a discrete number and unit of measurement
	🔀 A statement on whether measurements were taken from distinct samples or whether the same sample was measured repeatedly
	The statistical test(s) used AND whether they are one- or two-sided Only common tests should be described solely by name; describe more complex techniques in the Methods section.
	A description of all covariates tested
	🔀 A description of any assumptions or corrections, such as tests of normality and adjustment for multiple comparisons
	A full description of the statistical parameters including central tendency (e.g. means) or other basic estimates (e.g. regression coefficient) AND variation (e.g. standard deviation) or associated estimates of uncertainty (e.g. confidence intervals)
	For null hypothesis testing, the test statistic (e.g. <i>F</i> , <i>t</i> , <i>r</i>) with confidence intervals, effect sizes, degrees of freedom and <i>P</i> value noted <i>Give P values as exact values whenever suitable.</i>
\boxtimes	For Bayesian analysis, information on the choice of priors and Markov chain Monte Carlo settings
\boxtimes	For hierarchical and complex designs, identification of the appropriate level for tests and full reporting of outcomes
\boxtimes	\square Estimates of effect sizes (e.g. Cohen's d , Pearson's r), indicating how they were calculated
	Our web collection on statistics for biologists contains articles on many of the points above.

Software and code

Policy information about availability of computer code

Data collection

Flow cytometry data acquired using BD LSR Fortessa X-20 (BD Biosciences) with FACSDiva Software Version 8.0.1 (BD Biosciences). Multiplex immunohistochemistry was performed using MACSima imaging system Miltenyi Biotec. Spectral Flow cytometry was acquired using an Aurora spectral flow cytometer (5 lasers configuration, Cytek). Spinning-disk confocal intravital microscopy was performed using an Olympus BX51 (Olympus) upright microscope.

Data analysis

Flow cytometry analysis performed using FlowJo Software Version 10.8.1. and Graphpad Version 10.0. Multiplex immunohistochemistry pictures were first stitched and preprocessed using MACS iQ View Analysis Software (Miltenyi Biotec). Intravital microscopy images were processed and analyzed in Volocity 4.20. scRNAseq data was analyzed using CellRanger (v7.0) and Seurat (v4.3.0.1, R v4.3.1). Bulk-RNAseq data was analyzed using edgeR R package (version 3.34.0) and fgsea R package (version 1.18.0).

For manuscripts utilizing custom algorithms or software that are central to the research but not yet described in published literature, software must be made available to editors and reviewers. We strongly encourage code deposition in a community repository (e.g. GitHub). See the Nature Portfolio guidelines for submitting code & software for further information.

Data

Policy information about availability of data

All manuscripts must include a data availability statement. This statement should provide the following information, where applicable:

- Accession codes, unique identifiers, or web links for publicly available datasets
- A description of any restrictions on data availability
- For clinical datasets or third party data, please ensure that the statement adheres to our policy

scRNAseq data has been deposited on GEO under accession number GSE269104: Go to https://www.ncbi.nlm.nih.gov/geo/query/acc.cgi?acc=GSE269104

Research involving human participants, their data, or biological material

Policy information about studies with <u>human participants or human data</u>. See also policy information about <u>sex, gender (identity/presentation)</u>, <u>and sexual orientation</u> and <u>race, ethnicity and racism</u>.

Reporting on sex and gender	N/A
Reporting on race, ethnicity, or other socially relevant groupings	N/A
Population characteristics	N/A
Recruitment	N/A
Ethics oversight	N/A

Note that full information on the approval of the study protocol must also be provided in the manuscript.

Field-specific reporting

Please select the one belo	w that is the best fit for your research	If you are	e not sure, read the	appropriate sections before n	naking your selection.
X Life sciences	Behavioural & social sciences	Ecc	ological, evolutionar	y & environmental sciences	

For a reference copy of the document with all sections, see nature.com/documents/nr-reporting-summary-flat.pdf

Life sciences study design

All studies must disclose on these points even when the disclosure is negative.

Sample size

No statistical methods were used to pre-determine samples sizes. Sample sizes were empirically determined to optimize numbers based on

previous experience with equivalent experiments reported in previous publications (Khan et al. Cell 2020; Tran et al Nat Immunol 2024). A minimum sample size of 3 was always included for statistical analysis to be valid. Data distribution was assumed to be normal, but this was not

formally tested.

Blinding

Data exclusions No data points were excluded from analysis.

Replication

All experiments were reproduced independently two or three times for reproducibility of findings except for intravital microscopy, multiplex immunohistochemistry and RNA-seq as we considered the high output of data to be sufficient to corroborate our other reproducible findings.

Randomization All experiments involve mice or mouse-derived samples. Mice of the same sex were age-matched and randomly assigned prior to the

initiation of experiments.

Data collection and analysis were not performed blinded to the experimental conditions as experiments were all done by one researcher at a time.

Reporting for specific materials, systems and methods

We require information from authors about some types of materials, experimental systems and methods used in many studies. Here, indicate whether each material, system or method listed is relevant to your study. If you are not sure if a list item applies to your research, read the appropriate section before selecting a response.

Ma	terials & experimental systems	Methods
n/a	Involved in the study	n/a Involved in the study
	Antibodies	ChIP-seq
	Eukaryotic cell lines	Flow cytometry
\boxtimes	Palaeontology and archaeology	MRI-based neuroimaging
	Animals and other organisms	
\boxtimes	Clinical data	
\boxtimes	Dual use research of concern	
\boxtimes	Plants	

Antibodies

Antibodies used

Biotin-conjugated anti-Ter-119 (BD Biosciences; cat# 553672; clone Ter119; 1/100) Biotin-conjugated anti-CD11b (BD Biosciences; cat# 553309; clone M1/70; 1/100) Biotin-conjugated anti-CD5 (BD Biosciences; cat# 553018; clone 53-7.3; 1/100) Biotin-conjugated anti-CD4 (BD Biosciences; cat# 553045; clone RM4-5; 1/100) Biotin-conjugated anti-CD8a (BD Biosciences; cat# 553029; clone 53-6.7; 1/100) Biotin-conjugated anti-CD45R (BD Biosciences; cat# 553085; clone RA3-6B2; 1/100) Biotin-conjugated anti-CD45R (BD Biosciences; cat# 553125; clone RB6-8C5; 1/100) APC-Cy7-conjugated Streptavidin (BD Biosciences; cat# 554063; 1/100) APC-conjugated anti-cKit (Thermofisher; cat# 17-1171-82; clone 2B8; 1/100) PE-Cy7-conjugated anti-Sca-1 (Thermofisher; cat# 25-5981-82; clone D7; 1/100) eFluor450-conjugated anti-CD150 (Thermofisher; cat# 48-1502-82; clone mShad150; 1/100) BUV737-conjugated anti-CD48 (BD Biosciences; cat# 749666; clone HM48-1; 1/100) PE-conjugated anti-Flt3 (Thermofisher; cat# 12-1351-81; clone A2F10.1; 1/100) FITC-conjugated anti-CD34 (BD Biosciences: cat# 560238; clone RAM34: 1/100) BUV395-conjugated Streptavidin (BD Biosciences; cat# 564176; 1/100) BV421-conjugated anti-cKit (BD Biosciences; cat# 567818; clone 2B8; 1/100) PerCP-Cy5.5-conjugated anti-CD16/32 (Thermofisher; cat# 45-0161-82; clone 93; 1/100) BV711-conjugated anti-CD115 (BioLegend; cat# 135515; clone AFS98; 1/200) APC-conjugated anti-Ly6C (Thermofisher; cat# 17-5932-80; clone HK1.4; 1/200) AlexaFluor700-conjugated anti-Ly6G (BioLegend; cat# 127622; clone 1A8; 1/200) eFluor450-conjugated anti-CD11b (BD Biosciences; cat# 560456; clone M1/70; 1/200) PE-Cy7-conjugated anti-CD11c (BD Biosciences; cat# 561022; clone HL3; 1/200) PE-CF594-conjugated anti-SiglecF (BD Biosciences; cat# 562757; clone E50- 2440; 1/200) APC-conjugated anti-F4/80 (Thermofisher; cat#17-4801-82; clone BM8; 1/200) FITC-conjugated anti-Ly6C (BD Biosciences; cat 553104; clone AL-21; 1/200) PerCP-eFluor710 -conjugated anti-Ly6G (Thermofisher; cat# 46-9668-82; clone 1A8; 1/200) PE-conjugated anti-CD3 (Thermofisher; cat# 12-0031-81; clone 145-2C11; 1/200) PE-Cy7-conjugated anti-CD19 (Thermofisher; cat# 25-0193-81; clone eBio1D3 (1D3); 1/200) eFluor450-conjugated anti-CD4 (Thermofisher; cat# 48-0041-82; clone GK1.5; 1/200) AlexaFluor700-conjugated anti-CD8 (BD Biosciences; cat# 557959; clone 53-6.7; 1/200) APC-conjugated anti-CD45.1 (BD Biosciences; cat# 558701; clone A20; 1/200) FITC-conjugated anti-CD45.2 (BD Biosciences; cat# 553772; clone 104; 1/200) BUV395-conjugated anti-CD45.2 (BD Biosciences; cat# 564616; clone 104; 1/200) PerCP-conjugated anti-CD45 (Biolegend; cat# 103129; clone 30-F11;1/100) BUV395-conjugated anti-Ly6G (BD Biosciences; cat# 565964; clone 1A8;1/100) APC-conjugated anti-CD101 (Thermofisher; cat# 17-1011-82; clone Moushi101;1/100) PE-conjugated anti-CXCR2 (Biolegend; cat# 149303; clone SA044G4;1/100) BV711-conjugated anti-CXCR4 (Biolegend; cat# 146517; clone L276F12;1/100) BV480-conjugated anti-CD62L (BD Biosciences; cat# 746726; clone MEL-14;1/100) AlexaFluor700-conjugated anti-CD24 (Biolegend; cat# 101835; clone M1/69;1/100) BUV496-conjugated anti-CD11b (BD Biosciences; cat# 749864; clone M1/70;1/100) BUV563-conjugated anti-CD49d (BD Biosciences; cat# 741243; clone 9C10;1/100) BV570-conjugated anti-CD44 (Biolegend; cat# 103037; clone IM7;1/100) BV570-conjugated anti-CCR2 (BD Biosciences; cat# 747967; clone475301;1/100) BV785-conjugated anti-Ly6C (Biolegend; cat# 128041; clone HK1.4;1/100) BV650-conjugated anti-CD80 (BD Biosciences; cat# 563687; clone M18/2;1/100) BUV661-conjugated anti-MHCII (BD Biosciences; cat# 750280; clone M5/114;1/100) PE/Dazzle594 -conjugated anti-CD16 (Biolegend; cat# 158011; clone S17014E;1/100) AlexaFluor488 -conjugated anti-CD115 (Biolegend; cat# 135511; (clone AFS98;1/100) APC/Fire780 -conjugated anti-CD14 (Biolegend; cat# 1 123311; clone Sa14- 2;1/100) PE-conjugated anti-CD4 (Thermofisher; cat# 12-0042-82; clone RM4.5; 1/50) PE-conjugated anti-CD8 (Miltenyi Biotec; cat#130-128-228; clone REA601; 1/50) PE-conjugated anti-Ly6G (Miltenyi Biotec; cat# 130-102-934; clone 1A8; 1/50) APC-conjugated anti-CD11b (Miltenyi Biotec; cat# 130-113-239; clone M1/70; 1/50) PE-conjugated anti-CD14 (Biolegend; cat#123309; clone Sa14-2; 1/50) PE-conjugated anti-Ly6C (Miltenyi Biotec; cat# 130-128-235; clone REA796; 1/50) FITC-conjugated anti-CD45 (Miltenyi Biotec; cat# 130-110-803; clone REA737; 1/50) APC-conjugated anti-MHCII (Miltenyi Biotec; cat# 130-128-972; clone REA813; 1/50)

PE-conjugated anti-CXCR4 (Miltenyi Biotec; cat# 130-128-972; clone REA107; 1/50) APC-conjugated anti-CD62L (Miltenyi Biotec; cat#130-126-759; clone REA828; 1/50) PE-conjugated anti-CD49d (BD Biosciences; cat# 557420; clone MFR4.B; 1/50) PE-conjugated anti-CD31 (R&D; cat# AF3628; polyclonal; 1/50) PE-conjugated anti- LYVE-11 (R&D; cat# FAB2125P; clone 223322; 1/50)

FITC-conjugated anti- SMA (Miltenyi Biotec; cat# 130-123-363; clone REAL650; 1/50)

Validation

Antibodies are quality checked and validated by the respective manufacturers and informations regarding the validation can be found on the companies' websites. Each antibody has a recommended working concentration found on the associated Technical Data Sheet (eg Biolegend, suggested use of this reagent is ≤0.125 μg per million cells in 100 μl volume). Based on the recommended concentration, the antibody is titrated with cells of interest (lungs cells or PBMCs) for optimal performance by flow cytometry.

Eukaryotic cell lines

Policy information about cell lines and Sex and Gender in Research

MDCK cell line is from ATCC. Cell line source(s)

Authentication Growth rate and morphology of cells were checked frequently, but no profiling was performed.

All cells lines tested negative for mycoplasma. Mycoplasma contamination

Commonly misidentified lines (See ICLAC register)

No commonly misidentified cell lines were used.

Animals and other research organisms

Policy information about studies involving animals; ARRIVE guidelines recommended for reporting animal research, and Sex and Gender in Research

Laboratory animals

Six- to ten-week-old C57BL/6, CD45.1, Ifnar1-/-, IL1R-/-, Rag1-/-, RoRy-GFP/GFP, IFNARflox, B6.Cg-Tg(S100A8-cre), VertX(II10gfp) mice were purchased from Jackson Laboratories. All animals were housed and inbred at the animal facility of the Research Institute of McGill University under SPF conditions access to food and water, temperature of 21ºC (+/- 1ºC), relative humidity of 40-60%RH (+/-5%RH) and light cycle of 12 hours ON, 12 hours OFF (daily cycle). Six- to eight-week old females and males were used for experiments and were appropriately age- and sex-matched.

Wild animals

No wild animals were used.

Reporting on sex

All experiments with IAV infection were performed on female mice due to their higher susceptibility. Male or female mice were used for immunological phenotyping experiments and sex-matched accordingly as there were no observed differences in cellular composition.

Field-collected samples

No field-collected samples were used.

Ethics oversight

All experiments involving animals were approved by the McGill University Animal Care Committee (Permit # 2010-5860) in accordance with the guidelines set out by the Canadian Council on Animal Care.

Note that full information on the approval of the study protocol must also be provided in the manuscript.

Plants

Seed stocks	N/A

Novel plant genotypes

Ν

/A		

Authentication

/A			

Flow Cytometry

Plots

Confirm that:

- The axis labels state the marker and fluorochrome used (e.g. CD4-FITC).
- The axis scales are clearly visible. Include numbers along axes only for bottom left plot of group (a 'group' is an analysis of identical markers).
- All plots are contour plots with outliers or pseudocolor plots.
- A numerical value for number of cells or percentage (with statistics) is provided.

Methodology

Sample preparation

For intravascular staining of the lung, mice were anesthetized with isoflurane and intravenously injected with $1\mu g$ of CD45.2 (FITC-conjugated, BD) antibody in $100\mu l$ of sterile PBS. After two minutes, mice were euthanized, and lungs were harvested without perfusion. Lungs were treated with $100\ U$ of collagenase IV for $1\ h$ our at $37\ ^\circ$ C. Lungs were then filtered through a $70\mu m$ nylon mesh and red blood cells were lysed with an Ammonium-Chloride-Potassium lysing buffer. Blood was obtained through cardiac puncture, and directly stained with conjugated antibodies before red blood cells were lysed. Spleen cells were filtered through a $70\mu m$ nylon mesh and red blood cells were lysed. Bone marrow was obtained by snipping off the ends of the tibia and femur and spinning down the bones for $5\ seconds$ in a microtube. Peritoneal lavage was performed by inserting 5ml of cold sterile PBS into the peritoneal cavity, after a few minutes the PBS was retrieved with a $26G\ needle$. Samples were spun down and red blood cells were lysed. Cells were stained with viability dye eFluor- $506\ (Invitrogen)$ for $20\ minutes$ at $4\ ^\circ$ C, then stained with anti-CD16/32 (BD Bioscience) in $0.5\%\ BSA/PBS$ buffer to block non-specific binding with Fc receptors for $10\ minutes$ at $4\ ^\circ$ C. Cells were then stained for extracellular markers for $30\ min$ at $4\ ^\circ$ C.

Instrument

Samples were acquired on a BD LSR Fortessa X-20.

Software

Samples were collected using BD FACS Diva v8.0.1 and analyzed in Flow Jo v10.8.1.

Cell population abundance

The cell populations were sufficient for downstream analysis.

Gating strategy

Gating strategy for key cell populations are shown in Extended Data Figure 1.Cells were gated for FSC-A against SSC-A. Doublets were excluded using FSC-H against FSC-A. Viable CD45+ cells were gated, and within the viable CD45+ cells, cells were gated as CD11b, excluding SiglecF+ cells. CD11b and Ly6G double-positive cells were gated as neutrophils. Within the lineage-negative population, cells were gated as CD127+ and CD127-. Lin-CD127- population was further gated as LKS-defined as double positive for cKit and Sca-1, and cKit is gated as Sca- 1 negative and cKit positive.

Tick this box to confirm that a figure exemplifying the gating strategy is provided in the Supplementary Information.